

Shape evolution of compound droplet in combined presence of electric field and extensional flow

Somnath Santra,¹ Devi Prasad Panigrahi²,¹ Sayan Das²,¹ and Suman Chakraborty^{1,*}

¹*Department of Mechanical Engineering, Indian Institute of Technology Kharagpur, West Bengal 721302, India*

²*Department of Mechanical Engineering, Indian Institute of Technology Kanpur, Uttar Pradesh 208016, India*



(Received 19 January 2020; accepted 9 April 2020; published 1 June 2020)

Studies on compound droplet are of emerging importance in biology and engineering. Here, we bring out unique morphodynamics of a compound droplet as a consequence of interplay between an imposed electric field and an extensional flow. As compared to the deformation characteristics of compound droplet reported in the sole presence of extensional flow [Stone and Leal, *J. Fluid Mech.* **211**, 123 (1990)], our results implicate several nonintuitive findings on the dynamical evolution of the droplet. These exclusive new features include the interconversion of shape-evolution patterns of the compound droplet system contingent on the strength of background flow, electric field strength, electrophysical properties, and hitherto-unveiled post-breakup dynamics. Depending on these key parameters, in addition to three steady-state configurations, two new modes of droplet pinch-off are observed: Mode I: polar pinch-off; Mode II: equatorial pinch-off. Interestingly, the pinch-off time is found to vary nonmonotonically with the strength of the electric field. In sharp contrast to the extensional viscosity of a compound droplet in absence of other external fields [Stone and Leal, *J. Fluid Mech.* **211**, 123 (1990)], we show that the additional presence of electric field brings in an intricate dependence on the electrical properties of the inner droplet; a paradigm that is not prevalent in pure extensional flow.

DOI: [10.1103/PhysRevFluids.5.063602](https://doi.org/10.1103/PhysRevFluids.5.063602)

I. INTRODUCTION

Electrohydrodynamics (EHD) of droplets currently holds the attention of the scientific and industrial community because of its wide gamut of applications from natural to modern-day microfluidic processes [1–6]. While there are several appearances of single-phase droplets in flow processes, compound droplets also show significant importance in a growing number of novel applications. A compound droplet, which is also referred to as a double emulsion, has a unique nested structure, where an inner droplet is enclosed in a shell of an immiscible fluid. As the innermost droplet is not making any contact with the carrier phase, it has ubiquitous appearances in different applications including materials, pharmaceuticals, and microfluidics engineering. Some specific emerging applications include: microencapsulation of active ingredients [7,8], controlled release of drugs, vaccines and antigens [8,9], control over release of peptides, hormones like insulin [10], and removal of toxic material [11]. In recent times, compound droplets have also been used in distortion and recovery of white blood cells in the presence of background flow, where the compound droplet has been used to mimic the dynamics of a leukocyte. In such types of applications, the core (inner droplet) and the shell (outer droplet) denote the cell nucleolus and

*suman@mech.iitkgp.ac.in

cytoplasm, respectively [12–14]. In such scenarios, electric field can be used in controlling the dynamic evolution of the compound droplet system.

The deformation dynamics of a compound droplet in the sole presence of background flow has been well studied [15–20]. When such a double emulsion is subjected to a linear extensional flow, the two most important forces acting on the inner and outer interfaces are (i) viscous force which results in the deformation of the droplet and may ultimately lead to pinch-off of the droplet and (ii) restoring capillary force that helps the droplet in retaining its spherical configuration. The relative strength of the viscous force over the capillary force is denoted by capillary number (Ca). Lower values of Ca result in smaller deformation of the droplet, whereas higher values of it lead to higher deformation of the droplet. In a seminal study, Stone and Leal [15] have shown that, for a uniaxial extensional flow, the external fluid flow takes place from equators (directed along the axis of symmetry) to poles. This flow tries to deform the outer droplet into a prolate (the major axis of the ellipsoidal droplet align along the flow direction) configuration. At the same time, a biaxial flow is generated at the neighboring region of the inner droplet that deforms the inner droplet into an oblate (the major axis of the ellipsoidal droplet align perpendicular to the flow direction) configuration. Furthermore, their study also reveals that beyond a certain value of Ca (critical capillary number), the compound droplet system undergoes pinch-off. Later on, Qu and Yang [21] suggested that an increase in the size of the inner droplet also leads to the pinch-off of the compound droplet system.

With the advent of technology, the electric field can be used as an effective means of controlling the deformation dynamic of compound droplets. A wide gamut of literature is available where the electrohydrodynamics of a compound droplet is studied in the sole presence of a uniform electric field [22–26]. In brief, the application of electric field generates electrical stresses at the droplet interface that causes the deformation of the interface. The key parameters that regulate the sense and degree of deformation of the droplets via controlling the electrical stresses are the conductivity ratios, $R_{12} = \sigma_1/\sigma_2$, $R_{23} = \sigma_2/\sigma_3$ and the permittivity ratios, $S_{12} = \varepsilon_1/\varepsilon_2$, $S_{23} = \varepsilon_2/\varepsilon_3$ of the system [27,28], where σ and ε denote the conductivity and permittivity of the system and subscript 1, 2 and 3 symbolize the inner phase, outer phase and the suspending phase, respectively. In a related study, Behjatian and Esmaeeli [27] demonstrated that depending on conductivity and permittivity ratios, the outer-inner droplet of leaky dielectric double emulsion (having small but finite electrical conductivity) can show four different modes of deformation; i.e. prolate-prolate, prolate-oblate, oblate-oblate and oblate-prolate. In prolate and oblate configurations, the droplets are elongated along the direction of electric field and perpendicular to the direction of the electric field, respectively [27,28]. The presence of electric field also creates four different patterns of fluid motion in terms of external flow direction (pole to equator versus equator to pole), depending on the electrophysical properties of the system. In a recent study, Abbasi *et al.* [29] reported that, at higher electric field strength, the oblate-prolate (inner-outer interfaces) deformation undergoes pinch-off at the equator, whereas the prolate-oblate deformation of the interface cracks at the poles. In another study, Abbasi *et al.* [30] addressed the multimodal breakup of the compound droplet system for different electrophysical properties and volume fractions of the core liquid of the composite system.

From the above discussion, it is apparent that the interplay of electric field and extensional flow on the dynamics of a compound droplet has not been investigated by far. This situation, however, is not far from being involved and complicated, resulting in a paradigm that does not merely follow from a simple linear superposition of the EHD of the droplet in the uniform electric field and the hydrodynamics of the droplet in background extensional flow. The consequent nonlinearity and nontriviality essentially stem from the fact that toward obtaining a dynamical evolution of the droplet shape, electrical and hydrodynamic stresses at the droplet interface are mandated. However, for determining the distribution of electric potential and flow field, the knowledge of droplet shape is warranted. This triggers an interesting nonlinear coupling in the interfacial boundary conditions mediated by an unknown shape of the droplet during its dynamical evolution.

In addition to morphodynamic evolution, the understanding of the extensional rheology of a double emulsion is of significant importance in materials processing [31]. In several material processing systems including fiber spinning, extrusion and molding, a fluid element experiences extensional or

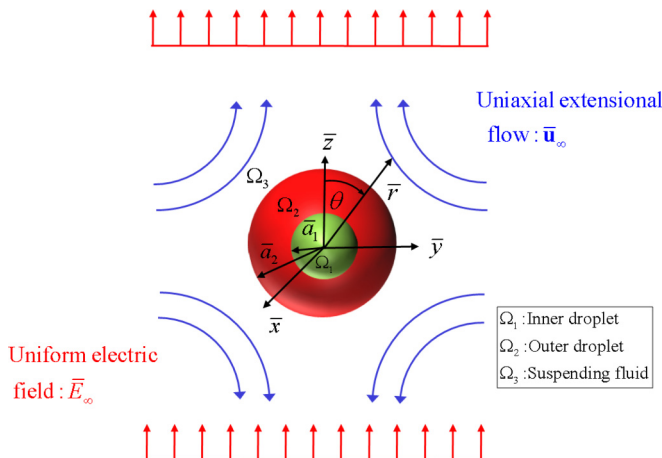


FIG. 1. Schematic representation of the compound droplet subjected to combined presence of uniform electric field and linear uniaxial extensional flow. The radius of the inner droplet and outer droplets are \bar{a}_1 and \bar{a}_2 .

elongation flow [32,33]. Furthermore, the rheological study provides useful information regarding the stability and internal microstructure of double emulsions. While the underlying consequences in the absence of electric field have been reported [15], the same cannot be straight-forward extended in presence of electric field, where the phenomenon is more complex and nontrivial.

Here, we bring out various aspects of morphodynamics and emulsion rheology, emerging from the combined consequence of uniform electric field and linear extensional flow, acting in tandem on a compound droplet. In sharp contrast to the reported results on extensional flow or electric field-driven flow alone, the present study unravels a plethora of unique nonintuitive findings, as a consequence of the deeply convoluted nonlinear coupling mediated of the respective driving influences, mediated by the dynamical evolution of the droplet shape mentioned as earlier. For instance, in the presence of electric field, we have obtained different shape-evolution patterns of the compound droplet system across electric capillary number-conductivity ratio spaces and electric capillary number-capillary number spaces; a paradigm hitherto being unveiled. We designate these patterns as: steady state I: Outer droplet is oblate shaped and inner droplet is prolate shaped; steady state II: Both the droplets are prolate shaped; steady state III: Outer droplet is prolate shaped and the inner droplet is oblate shaped. Besides that, two different modes of droplet pinch-off are also observed: Mode I: polar pinch-off; Mode II: equatorial pinch-off. The pinch-off time is also found to be a strong function of electric field strength, with exclusive monotonic or nonmonotonic dependences on the electric field. Further, contrary to the sole effect of uniaxial extensional flow, after pinch-off, the interface of the outer shell again gets reunited in the presence of electric field and forms a cylindrical inner droplet. As time evolves, this inner droplet undergoes midpoint pinch-off creating two spherical inner daughter droplets, leading to unique post pinch-off dynamics. The size of the daughter droplet reduces as the strength of the electric field increases. Finally, in presence of the electric field, the extensional viscosity of the droplet turns out to be strongly dependent on the electrophysical properties of the inner droplet, in addition to the radius ratio and the viscosity ratio, with variations in a nontrivial pattern.

II. PROBLEM FORMULATION

Figure 1 illustrates the physical setup, where a dielectric neutrally buoyant compound droplet is suspended in another dielectric and immiscible fluid. The fluids are Newtonian in nature. The system experiences the combined presence of the uniform electric field, $\vec{E}_\infty = \bar{E}_\infty \mathbf{e}_z$ (here, \bar{E}_∞ is

the magnitude of electric field and \mathbf{e}_z is the unit vector along the z axis) and linear extensional flow, $\bar{\mathbf{u}}_\infty = \bar{\Gamma}_\infty \cdot \bar{\mathbf{x}}$, where $\bar{\mathbf{x}}$ symbolizes the position vector and $\bar{\Gamma}_\infty$ denotes the far-field strain rate tensor, read as

$$\bar{\Gamma}_\infty = \frac{\bar{S}_R}{2} \begin{bmatrix} -1 & 0 & 0 \\ 0 & -1 & 0 \\ 0 & 0 & 2 \end{bmatrix}, \quad (1)$$

where \bar{S}_R is the shear rate. The radii of the undeformed inner and outer droplets are \bar{a}_1 and \bar{a}_2 , respectively. We have used subscripts 1, 2, and 3 for inner droplet (inner phase), outer droplet (outer phase), and suspending phase (ambient fluid), respectively. The viscosity, electrical conductivity and electrical permittivity of the i th fluids ($i = 1, 2, 3$) are μ_i , σ_i , and ε_i , respectively. However, subscript “ ij ” has been used to denote the interface between i th and j th fluid. The interfacial tension between the i th and j th fluids is symbolized by γ_{ij} . Under the integrated influence of extensional flow and uniform electric field, both the inner and outer droplets deform into the ellipsoidal configuration, that can be expressed in the form $\bar{r}_s(\theta) = \bar{a}[1 + \bar{f}(\theta)]$, where the deviation in the droplet shape from a perfect sphere (having undeformed radius \bar{a}) is denoted by $\bar{f}(\theta)$. Determining $\bar{f}(\theta)$ is one of our primary goals. Another important aspect of our study is to find out the effective extensional viscosity (μ_{ext}) of a dilute double emulsion. For the current investigation, we have taken a spherical polar coordinate system (\bar{r}, θ) anchored at the centroid of the outer droplet. Here, dimensional and nondimensional quantities are introduced with and without bars, respectively. In every stage of our analysis, we have expressed all the quantities in their nondimensional form, unless stated otherwise.

For the purpose of nondimensionalization, we have chosen the following scales: length $\sim \bar{a}_2$, velocity $\sim \bar{S}_R \bar{a}_2$, electric field $\sim \bar{E}_\infty$, viscous stress $\sim \mu_3 \bar{S}_R$, and electric stress $\sim \varepsilon_3 \bar{E}_\infty^2$. Using the present nondimensional scheme, we have identified some dimensionless numbers and property ratios: electric capillary number, $Ca_E = \varepsilon_3 \bar{E}_\infty^2 \bar{a}_2 / \gamma_{23}$ (which symbolizes the relative strength of electric stress in comparison to the capillary stress), Reynolds number, $Re = \rho_3 \bar{S}_R \bar{a}_2^2 / \mu_3$ (which stands for the relative strength of inertia force over viscous force), capillary number, $Ca = \mu_3 \bar{S}_R \bar{a}_2 / \gamma_{23}$ (which symbolizes the ratio of viscous stress and capillary stress), Mason number, $M = Ca_E / Ca$ (which denotes the strength of the electric stress relative to the viscous stress), radius ratio, $K = \bar{a}_1 / \bar{a}_2$, viscosity ratio, $\lambda_{12} = \mu_1 / \mu_2$ and $\lambda_{23} = \mu_2 / \mu_3$, conductivity ratio, $R_{12} = \sigma_1 / \sigma_2$ and $R_{23} = \sigma_2 / \sigma_3$, and permittivity ratio, $S_{12} = \varepsilon_1 / \varepsilon_2$ and $S_{23} = \varepsilon_2 / \varepsilon_3$.

A. Assumptions

The assumptions made for the simplification of the present problem are as follows: (i) the viscous and pressure forces are dominating over the inertia forces. Hence the value of Re ($Re = \rho_3 \bar{S}_R \bar{a}_2^2 / \mu_3$) can be assumed to be very low ($Re \sim 0$), (ii) the system is considered to be neutrally buoyant that means the density of the three phases are the same ($\rho_1 = \rho_2 = \rho_3$), (iii) the effect of charge convection has been neglected which indicates that the value of the electric Reynolds number ($Re_E = \varepsilon_3 \bar{S}_R / \sigma_3$) is very small ($Re_E \ll 1$). An example of such a droplet-based fluidic system is a composite system, where the inner and outer radii are 2 and 4 mm, respectively. The composite system is suspended in another dielectric medium under an electric field having a strength of 1×10^5 V/m, where the inner droplet and ambient fluid are silicon oil and the outer droplet is made of oxidized castor oil. The properties of the inner droplet (or the ambient fluid) are: permittivity (ε) = 2.44×10^{-11} F/m, conductivity (σ) = 3.33×10^{-11} S/m, viscosity (μ) = 12 Pa s, and density (ρ) = 980 kg/m^3 , whereas the properties of outer fluid phases are $\varepsilon = 10^{-9}$ F/m, $\sigma = 5.57 \times 10^{-11}$ S/m, $\mu = 6.5$ Pa s and $\rho = 980 \text{ kg/m}^3$. The surface tension of the fluid-fluid interface is 5.5 mN/m at a room temperature of 32°C. These fluid properties are reported in the experimental study of Torza *et al.* [34]. Based on the reported fluid properties, the obtained nondimensional numbers are $Re_E \sim O(10^{-2})$ and $Re \sim O(10^{-4})$.

B. Governing equations and boundary conditions

According to the leaky dielectric theory proposed by Taylor [35], we have assumed that the free charges instantaneously move to the interface and the bulk remains free of charge. Under this assumption, the electrostatic problem is governed by the Laplace equation and the solution of this provides us the distribution of electric potential for the i th ($i = 1, 2, 3$) fluid. The equation is read as [36]

$$\nabla^2 \phi_i = 0, \quad (2)$$

where ϕ_1 , ϕ_2 , and ϕ_3 denote the electric potential for the inner, annular, and ambient fluid, respectively.

At the center of the inner droplet, the electric potential is finite and bounded. Far away from the outer interface, the electric potential becomes identical to the externally imposed potential,

$$\phi_3 = -\mathbf{E}_\infty \cdot \mathbf{r} \quad \text{as } r \rightarrow \infty. \quad (3)$$

At the two deformed interfaces, the electric potential is continuous and can be read as

$$[\phi_i]_{\Pi_{ij}} = [\phi_e]_{\Pi_{ij}} \quad \text{at } r = r_{\Pi_{ij}}(\theta, t). \quad (4)$$

Here, $\nabla r = r_{\Pi_{ij}}(\theta)$ denotes the radial position of the deformed interfaces and θ is the cylindrical polar angle. Π_{ij} symbolizes the interface of the fluids i and j and $[\]_{\Pi_{ij}}$ refers to the evaluation of the bracketed quantity at the interface Π_{ij} . In addition, at the interface Π_{ij} , the electric potential satisfies the following boundary condition

$$[R_{ij} \nabla \phi_i \cdot \mathbf{n}_{ij}]_{\Pi_{ij}} - [\nabla \phi_j \cdot \mathbf{n}_{ij}]_{\Pi_{ij}} = \text{Re}_E \nabla_s \cdot (q_s \mathbf{u}_s) \quad \text{at } r = r_{\Pi_{ij}}(\theta), \quad (5)$$

where \mathbf{n}_{ij} symbolizes the outward normal unit vector at the deformed interfaces of the droplets and is given by $\mathbf{n}_{ij} = \nabla(r - r_{\Pi_{ij}})/|\nabla(r - r_{\Pi_{ij}})|$. The left-hand side of Eq. (5) denotes the Ohmic conduction and the right side symbolizes the convection of free charges. \mathbf{u}_s and ∇_s denote the surface velocity and surface gradient operator, respectively. ∇_s is expressed as $\nabla_s = \nabla_{ij} - \mathbf{n}_{ij}(\mathbf{n}_{ij} \cdot \nabla_{ij})$. q_s is the surface charge density which is computed as $q_s = (S_{ij} \nabla \phi_i - \nabla \phi_j) \cdot \mathbf{n}_{ij}$ [36,37]. In our present analysis, we have assumed that the value Re_E is very small ($\text{Re}_E \ll 1$) (refer to Sec. I of the Supplemental Material [38] for justification of the assumption). Therefore, Eq. (5) is reduced to

$$[R_{ij} \nabla \phi_i \cdot \mathbf{n}_{ij}]_{\Pi_{ij}} - [\nabla \phi_j \cdot \mathbf{n}_{ij}]_{\Pi_{ij}} = 0 \quad \text{at } r = r_{\Pi_{ij}}(\theta). \quad (6)$$

Under creeping flow condition ($\text{Re} \sim 0$), the continuity and the Stokes equations govern the fluid flow problem and these equations are read as

$$\nabla \cdot \mathbf{u}_i = 0, \quad \nabla p_i - \lambda_{ij} \nabla^2 \mathbf{u}_i = 0, \quad (7)$$

where \mathbf{u} and p represent the velocity field and pressure field, respectively. Due to the symmetric nature of the flow field and electric field about the z -axis, we have used the stream function approach to simplify our theoretical analysis. In terms of stream function (ω), the Stokes equation for i th ($i = 1, 2$, and 3) phase is written as

$$\ell^2(\ell^2 \omega_i) = 0, \quad (8)$$

where ℓ^2 denotes the second-order linear operator, expressed as $\ell^2 = \frac{\partial^2}{\partial r^2} + \left[\frac{(1-\eta^2)}{r^2}\right] \frac{\partial}{\partial \eta^2}$. Here, $\eta = \cos(\vartheta)$ symbolizes the transformed polar co-ordinate.

The velocity field must be bounded in the interior of the inner droplet. Far away from the compound droplet system, the velocity field must be similar to the undisturbed imposed flow field. This far-field condition can be expressed as

$$r \rightarrow \infty, \quad \mathbf{u}_3 \rightarrow \bar{\mathbf{u}}_\infty. \quad (9)$$

At the deformed interfaces, the velocity field fulfills the no penetration and no-slip boundary conditions which can be expressed as

$$\left. \begin{aligned} [\mathbf{u}_i]_{\Pi_{ij}} &= [\mathbf{u}_j]_{\Pi_{ij}} \quad \text{at } r = r_{\Pi_{ij}}(\theta) \\ [\mathbf{u}_i \cdot \mathbf{n}_{ij}]_{\Pi_{ij}} &= [\mathbf{u}_j \cdot \mathbf{n}_{ij}]_{\Pi_{ij}} \quad \text{at } r = r_{\Pi_{ij}}(\theta) \end{aligned} \right\} \quad (10)$$

Furthermore, the pressure and velocity fields also satisfy the interfacial stress balance equation which consists of electric stress, hydrodynamic stress and capillary stress. This equation is represented in the following form:

$$[(\tau_j^H + M\tau_j^E) \cdot \mathbf{n}_{ij}]_{S_{ij}} - [(\tau_i^H + M\tau_i^E) \cdot \mathbf{n}_{ij}]_{S_{ij}} = \frac{1}{\text{Ca}}(\nabla \cdot \mathbf{n}_{ij})\mathbf{n}_{ij} \quad \text{at } r = r_{S_{ij}}(\theta). \quad (11)$$

Here τ^H and τ^E symbolize the hydrodynamic and electric stress tensors, respectively.

C. Small-deformation perturbation analysis

From the above mathematical formulation, it becomes evident that the governing equations along with its boundary conditions are highly coupled and nonlinear in nature. The source of nonlinearities arising in the present problem is due to the deformation of the fluid-fluid interfaces. A close inspection into Eq. (5) reveals the fact that the electric potential distribution is dependent on the shape-deformation of the interface. However, on analyzing Eq. (11), it becomes clear that the deformed shape of the droplet depends on the electric stresses which are dictated by the distribution of the electric potential. Therefore, the electrodynamics of the problem is highly coupled with the shape deformation. This limits our analytical solution to the case when the interfacial deformation is small. We have employed the method of regular perturbation where we have taken Ca to be the perturbation parameter [39–41]. Keeping this in mind, we have used the following expansion for a generic field variable χ [39,42].

$$\chi = \chi^{(0)} + \text{Ca}\chi^{(\text{Ca})} + \text{Ca}^2\chi^{(\text{Ca}^2)} + O(\text{Ca}^3). \quad (12)$$

Here, $\chi^{(0)}$ symbolizes the leading-order term of χ (when shape deformation is absent) and $\chi^{(\text{Ca})}$ stands for the first-order correction arising due to shape deformation. In the present analytical solution, we have considered droplet shape corrected up to $O(\text{Ca}^2)$ and performed comparisons of the same with numerically obtained solutions.

III. ASYMPTOTIC SOLUTION FOR SMALL SHAPE DEFORMATION

A. Droplet shape

The $O(\text{Ca})$ correction to the shape of the inner and outer droplets are given by

$$f_{12}^{(\text{Ca})} = L_{12}^{(\text{Ca})}P_2[\cos(\theta)]; \quad f_{23}^{(\text{Ca})} = L_{23}^{(\text{Ca})}P_2[\cos(\theta)]. \quad (13)$$

Here, $f_{12}^{(\text{Ca})}$ and $f_{23}^{(\text{Ca})}$ represent the leading order deviations in the shape of the inner and outer droplets, respectively. The coefficients $L_{12}^{(\text{Ca})}$ and $L_{23}^{(\text{Ca})}$ are expressed as

$$L_{12}^{(\text{Ca})} = \Phi_1(R_{ij}, S_{ij}, \lambda_{ij}, M, K); \quad L_{23}^{(\text{Ca})} = \Phi_2(R_{ij}, S_{ij}, \lambda_{ij}, M, K); \quad (ij) \in \{12, 23\}. \quad (14)$$

The $O(\text{Ca}^2)$ correction to the droplet shapes are obtained as

$$\left. \begin{aligned} f_{12}^{(\text{Ca}^2)} &= L_{12}^{(\text{Ca}^2)}P_2[\cos(\theta)] + L_{14}^{(\text{Ca}^2)}P_4[\cos(\theta)] \\ f_{23}^{(\text{Ca}^2)} &= L_{22}^{(\text{Ca}^2)}P_2[\cos(\theta)] + L_{24}^{(\text{Ca}^2)}P_4[\cos(\theta)] \end{aligned} \right\} \quad (15)$$

where

$$L_{12}^{(\text{Ca}^2)} = \Phi_3(R_{ij}, S_{ij}, \lambda_{ij}, M, K); \quad L_{14}^{(\text{Ca}^2)} = \Phi_4(R_{ij}, S_{ij}, \lambda_{ij}, M, K); \quad (ij) \in \{12, 23\}, \quad (16)$$

$$L_{22}^{(\text{Ca}^2)} = \Phi_5(R_{ij}, S_{ij}, \lambda_{ij}, M, K); \quad L_{24}^{(\text{Ca}^2)} = \Phi_6(R_{ij}, S_{ij}, \lambda_{ij}, M, K); \quad (ij) \in \{12, 23\}. \quad (17)$$

The functions Φ_1, ϕ_2 , etc ... appearing in Eqs. (14), (16), and (17) have very lengthy algebraic expressions. Thus, we have not written the detailed expressions here. MAPLE files containing these expressions would be made available upon request.

Therefore, the deformed shape of the inner droplet can be expressed as

$$r_{12} = K[1 + \text{Ca}f_{12}^{(\text{Ca})} + \text{Ca}^2(\alpha_1 + f_{12}^{(\text{Ca}^2)})]. \quad (18)$$

The term α_1 appearing in Eq. (18) is introduced to conserve the total volume of the inner droplet, $\alpha_1 = -\frac{(L_{12}^{(\text{Ca})})^2}{5}$. Similarly, the deformed shape of the outer droplet is given by

$$r_{23} = [1 + \text{Ca}f_{23}^{(\text{Ca})} + \text{Ca}^2(\alpha_2 + f_{23}^{(\text{Ca}^2)})], \quad (19)$$

where $\alpha_2 = -\frac{(L_{23}^{(\text{Ca}^2)})^2}{5}$ is introduced for the purpose of volume conservation of the outer droplet. Finally, the deformation parameter D_{ij} is defined as $D_{ij} = \frac{r_{ij}(\theta=0) - r_{ij}(\theta=\pi/2)}{r_{ij}(\theta=0) + r_{ij}(\theta=\pi/2)}$. Throughout the manuscript, $D_{\infty,ij}$ [$ij \in (12, 23)$] has been used to denote the steady-state deformation of the droplet. The results of the present study indicate that the deformation of a compound droplet cannot be understood simply as a linear superposition of the deformation due to an external electric field and an imposed extensional flow.

B. Extensional emulsion rheology

In this section, we are interested to derive the effective extensional viscosity of the double emulsion under combined effect of electric field and background uniaxial extensional flow. The presence of electric field alters the droplet shape and flow field. This perturbed flow field and droplet shape, in turn, affect the rheological behavior of the double emulsion under uniaxial extensional flow. The suspension stress of a double emulsion experiencing linear flow can be expressed as [43]

$$\Sigma = -p\mathbf{I} + 2\Gamma + \Sigma^{(d)}, \quad (20)$$

where $\Sigma^{(d)}$ is the stresslet tensor and it can be expressed in the following format [43]:

$$\Sigma^{(d)} = \frac{3\nu}{4\pi} \int_{\Pi_{23}} \left[\frac{1}{2} \left\{ (\tau_3^H \cdot \mathbf{n})\mathbf{r} + [(\tau_3^H \cdot \mathbf{n})\mathbf{r}]^T - \frac{2}{3}\mathbf{I}(\tau_3^H \cdot \mathbf{n}) \cdot \mathbf{r} \right\} - [\mathbf{u}_3\mathbf{n} + (\mathbf{u}_3\mathbf{n})^T] \right] d\Pi_{12}, \quad (21)$$

where ν denotes the volume fraction. Since we have considered dilute emulsion, the magnitude of ν is much lesser than 1. For quantifying different effects, we have defined a dimensionless extensional viscosity μ_{ext} , expressed as

$$\mu_{\text{ext}} = \frac{\bar{\Sigma}_{zz} - \bar{\Sigma}_{xx}}{\dot{S}_R} = \frac{\bar{\Sigma}_{zz} - \bar{\Sigma}_{yy}}{\dot{S}_R}. \quad (22)$$

In Eq. (22), the dimensional component of stress can be denoted as $\bar{\Sigma}_{ij} = \mu_e \dot{S}_R \Sigma_{ij}$. After substituting relevant terms, we have obtained the extensional viscosity ratio in the following form

$$\eta_{\text{ext}} = \frac{\mu_{\text{ext}}}{\mu_e} = \eta_{\text{ext}}^{(0)} + \text{Ca} \eta_{\text{ext}}^{(\text{Ca})}, \quad (23)$$

where $\eta_{\text{ext}}^{(0)}$ denotes the leading order extensional viscosity obtained by neglecting the effect of shape deformation. However, the term $\eta_{\text{ext}}^{(\text{Ca})}$ is obtained by considering the effect of shape deformation.

The terms $\eta_{\text{ext}}^{(0)}$ and $\eta_{\text{ext}}^{(\text{Ca})}$ are read as

$$\eta_{\text{ext}}^{(0)} = \Phi_7(R_{ij}, S_{ij}, \lambda_{ij}, M, K), \quad \eta_{\text{ext}}^{(\text{Ca})} = \Phi_8(R_{ij}, S_{ij}, \lambda_{ij}, M, K), \quad (ij) \in (12, 23). \quad (24)$$

Because of very lengthy and complicated algebraic expressions of ϕ_7 and ϕ_8 appearing in Eq. (24), we have not explicitly stated the detailed expressions here. MAPLE files containing these expressions of functions ϕ_7 and ϕ_8 appearing in Eq. (24) would be made available upon request.

IV. NUMERICAL APPROACH

For arresting the important features of droplet dynamics beyond the small deformation limit, we have performed numerical simulations. For simplification, we have considered a two-component composite droplet system, where the inner droplet and the suspending fluid are identical. Thus, the system reduces to a two-phase interfacial flow system. Typical examples of such types of systems are water-oil-water and oil-water-oil compound droplets [44]. For numerical simulations, we have exploited the phase field model for tracking the interface of the binary fluid system. Phase field model is developed based on Cahn-Hilliard and Navier-Stokes equations. The former one is derived based on the principle of energy minimization of a system that consists of two incompressible as well as immiscible fluids and represented in the dimensionless form [45–48] as follows:

$$\frac{\partial \psi}{\partial t} + \mathbf{u} \cdot \nabla \psi = \frac{1}{\text{Pe}} \nabla \cdot M_\psi (\nabla G), \quad \text{where} \quad G = \frac{1}{\text{Cn}} (\psi^3 - \psi) - \text{Cn} \nabla^2 \psi. \quad (25)$$

Here M_ψ and G denote the phase field mobility parameter and chemical potential, respectively, in their nondimensional forms. Another important parameter appearing in the expression of G is the Cahn number (Cn). It stands for the order of the magnitude of the nondimensional thickness of the diffusive interface and reads as $\text{Cn} = \bar{\zeta}/\bar{a}_2$ [46], where $\bar{\zeta}$ regulates the interfacial thickness and a_2 is the radius of the outer droplet. ψ is termed as phase field parameter that is defined in the entire domain and acquires specific values for the identification of different fluid elements. It acquires the value of -1 in the inner droplet and $+1$ in the outer fluid domain. The electric potential satisfies the Poisson's equation in the following form

$$\nabla \cdot (\varepsilon \nabla \phi) = q_v, \quad (26)$$

where q_v is the volumetric charge density and it is obtained by solving the charge transport equation in the following form

$$\nabla \cdot (\varepsilon \nabla \phi) = -q_s; \quad \text{Re}_E \left(\frac{\partial q_v}{\partial t} + \nabla \cdot (q_v \mathbf{u}) \right) = \nabla \cdot (\sigma \nabla \phi), \quad (27)$$

where σ and ε denote the conductivity and permittivity of the fluid, respectively. In terms of the phase field parameter, these properties are expressed in the following form:

$$\sigma = \frac{(1 + \psi)}{2} R_{ij} + \frac{(1 - \psi)}{2}; \quad \varepsilon = \frac{(1 + \psi)}{2} S_{ij} + \frac{(1 - \psi)}{2} \left. \right\}, \quad \text{where} \quad [i, j \in (1, 3)]. \quad (28)$$

As we have considered that Re_E is much smaller than unity (the justification of our assumption is given in Sec. I of the Supplemental Material [38]), the governing equation for electric potential reduces to

$$\text{Leaky dielectric: } \nabla \cdot (\sigma \nabla \phi) = 0. \quad (29)$$

The distribution of velocity and pressure field is achieved by solving the continuity and Cahn-Hilliard-Navier-Stokes equation. The phase field and electrohydrodynamics are coupled through the latter equation. In dimensionless format, the continuity and Cahn-Hilliard-Navier-Stokes equation are read as

$$\nabla \cdot \mathbf{u} = 0, \quad \text{Re} \left(\frac{\partial \mathbf{u}}{\partial t} + \nabla \cdot (\mathbf{u} \mathbf{u}) \right) = -\nabla p + \nabla \cdot [\{\nabla \mathbf{u} + (\nabla \mathbf{u})^T\}] + \frac{1}{\text{Ca}} G \nabla \psi + M \mathbf{F}^E. \quad (30)$$

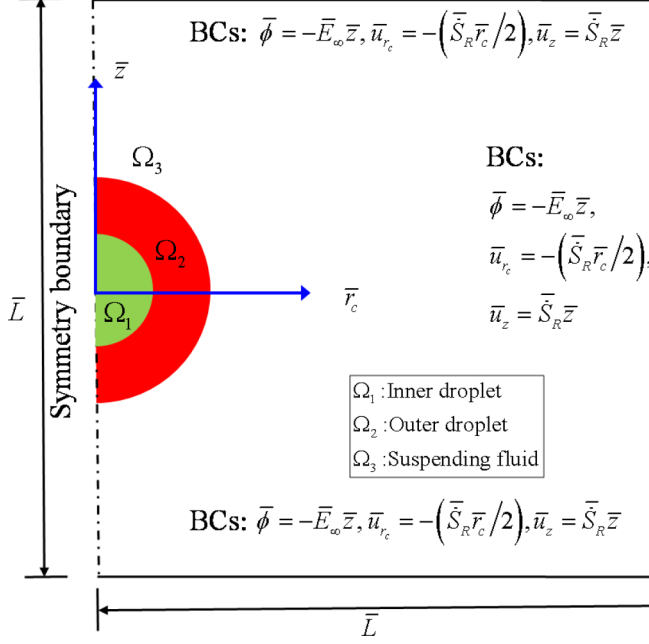


FIG. 2. Schematic representation of the problem set up. The computational domain is axisymmetric with rectangular size $\bar{L} \times \bar{L}$. A cylindrical coordinate system (\bar{r}_c, \bar{z}) is considered and attached to the droplet center.

The simulation is performed on a 2D axisymmetric domain in a cylindrical coordinate system (r_c, z) . Figure 2 shows the relevant boundary conditions employed in the numerical investigation. For neglecting the effect of channel confinement, we have considered a large value of L ($L = 10$). Furthermore, to neglect the effect of fluid inertia, we have considered a small value of Re ($Re = 0.01$). For high deformation, the outer interface of the compound droplet ruptures, releasing the inner droplet into the suspending fluid. This phenomenon is defined as pinch-off of a compound droplet and the time of interfacial rupture is termed as pinch-off time. It is worth mentioning that, in numerical modeling, the exact pinch-off time relies on the thickness of the interfacial regions undergoing topological changes. For a droplet-based microfluidic system, which is of interest in the present analysis, we resolve the interfaces down to a very small but finite thickness, comparable to real interface [$\sim O(10^{-2} \mu\text{m})$]. As the interfacial thickness imitates reality, we can conclude that the pinch-off time is close to the real one. In the present study, we have denoted pinch-off time by $t_{\text{pinch off}}$. For ensuring that the findings of the numerical analysis do not depend on the size of the grid element, a grid independence study has also been made (refer to Sec. II of Supplemental Material [38]).

V. RESULTS AND DISCUSSIONS

A. Model validation study

1. Comparison between the present and existing results

First, for checking the applicability of the present model, we have carried out model validation tests.

We have compared the results obtained from our numerical simulations and small deformation asymptotic analysis with those reported in the classical work of Stone and Leal [15] as shown in Fig. 3(a), where they have numerically investigated the deformation of a concentric compound droplet which is exposed to an imposed linear flow. From Fig. 3(a), we have observed that the

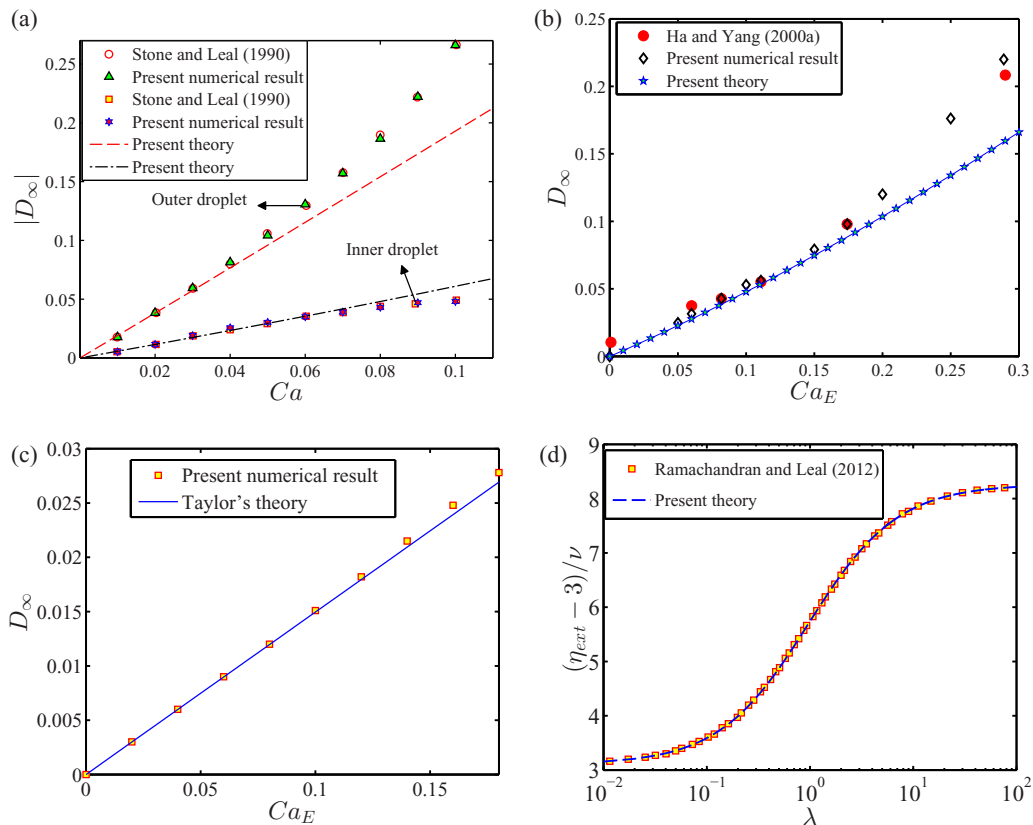


FIG. 3. (a) Alteration of D_∞ (steady-state deformation) with Ca (capillary number) for compound droplet when Re (Reynolds number) = 0.01, K (radius ratio) = 0.5 and λ_{12} (viscosity ratio) = λ_{32} (viscosity ratio) = 1. (b) Alteration of D_∞ with Ca_E (electric capillary number) for a single droplet at $Re = 0.01$, R (conductivity ratio) = 10, S (permittivity ratio) = 1.37, λ (viscosity ratio) = 0.874. (c) Variation of D_∞ with Ca_E for a single droplet having $R = 2$, $S = 1$, $\lambda = 10$, $Re = 0.01$. (d) Variation of effective extensional viscosity of dilute emulsion of single droplets with λ for a droplet having $Ca = 0.1$. For single droplet λ_{ij} [(ij) \in {12, 23}] is expressed as λ . 1, 2, and 3 are used to denote the inner fluid, the outer fluid, and the suspending fluid, respectively.

variation of steady-state deformation with Ca for both the inner and outer droplets as obtained from our analytical solution matches well with the results published by Stone and Leal [15] for lower values of Ca . With the rise in the values of Ca , the analytical results under-predict the deformation for both the inner and outer droplets. However, our numerical results predict the magnitude of deformation very well, even in the regime of higher deformation. Furthermore, we have performed yet another comparison of the steady-state deformation parameter of a single droplet subjected to the uniform electric field with the experimental results of Ha and Yang [49] as depicted in Fig. 3(b). Here, we have compared our numerical and analytical results with the experimental findings of Ha and Yang [49] for the limiting case when the radius ratio of the compound droplet system tends to zero (single droplet). Here also, we have obtained an acceptable agreement between our numerical results and the results obtained from the experimental study of Ha and Yang [49]. However, the analytical results show good agreement only at lower values of Ca_E (< 0.15). In Fig. 3(c), we have again compared our results with the analytical result of Taylor [35] on the deformation of the single droplet in the presence of uniform electric field and we have found an excellent agreement

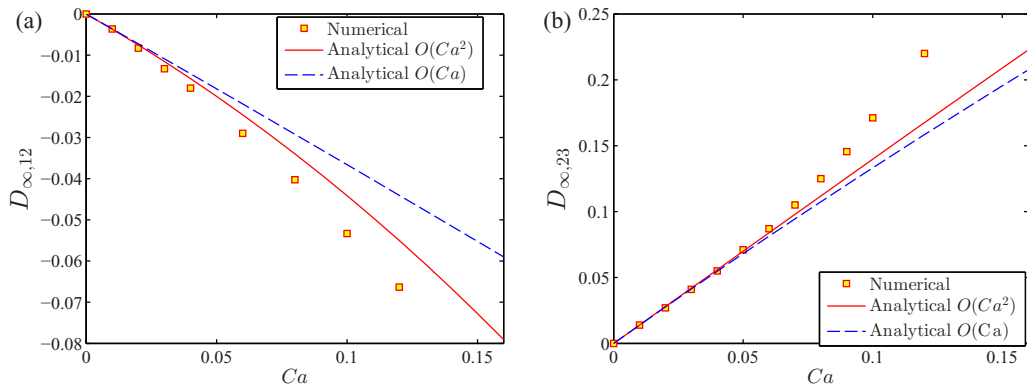


FIG. 4. Alteration of D_{∞} (steady-state deformation) with Ca (capillary number) for (a) inner droplet (b) outer droplet of a system with $(S_{23}, R_{23}) = (2, 0.5)$ and $(S_{12}, R_{12}) = (0.5, 2)$. Other used parameters are Re (Reynolds number) = 0.01, λ_{12} (viscosity ratio) = λ_{32} (viscosity ratio) = 1, M (Mason number) = 1, K (radius ratio) = 0.5. Here, R_{ij} (conductivity ratio) = σ_i/σ_j , S_{ij} (permittivity ratio) = $\varepsilon_i/\varepsilon_j$, and λ_{ij} (viscosity ratio) = μ_i/μ_j , where $(ij) \in \{12, 23\}$. 1, 2, and 3 are used to denote the inner fluid, outer fluid, and suspending fluid, respectively. The viscosity, electrical conductivity, and electrical permittivity are denoted by μ , σ , and ε , respectively.

between them. We have also performed another model validation study on the variation of effective extensional viscosity of dilute emulsion of single droplet between our analytical result and the result of Ramachandran and Leal [50] as shown in Fig. 3(d). Here λ denotes the ratio of viscosities of the single droplet and the suspending fluid. This figure shows an exact matching between the results. In the study of Ramachandran and Leal [50], the effect of slip has been considered. However, for validation purposes, we have put the value of the slip factor as zero in the expression of extensional viscosity as proposed by Ramachandran and Leal [50].

2. Comparison between present numerical and analytical results

In Fig. 4, we have shown a comparison between our analytical and numerical results. Figures 4(a) and 4(b) depict the alteration of steady-state deformation with capillary number for the inner and outer droplets of a concentric leaky dielectric system with $(S_{23}, R_{23}) = (2, 0.5)$ and $(S_{12}, R_{12}) = (0.5, 2)$. From the figure, it can be concluded that the numerical and the analytical results (both the leading order linear theory and higher-order nonlinear theory) depict very good agreement with each other for lower values of capillary number (Ca). However, at comparatively higher values of Ca , the higher-order nonlinear theory depicts a better match with the numerical results as compared to the leading order linear theory. However, as we increase the values of Ca , we observe that the higher-order nonlinear theory also under-estimates the deformation both for inner and outer droplets.

Therefore, we have decided to use the higher-order asymptotic solution to study the deformation characteristic and emulsion rheology of the system in a low deformation limit. Beyond the range of the validity of the asymptotic solution, we have used numerical simulations to address large deformation.

B. Deformation characteristics

1. Influence of electric field on the steady-state deformation of the droplet

Figure 5 depicts the variation of steady-state deformation parameter with Mason number (or Ca_E as Ca is fixed) in low deformation limit for a pair of leaky dielectric systems. For studying the deformation dynamics in low deformation limit, we have used the low-deformation asymptotic solution. Figure 5(a) depicts that the inner droplet deforms into an oblate shape in the sole presence

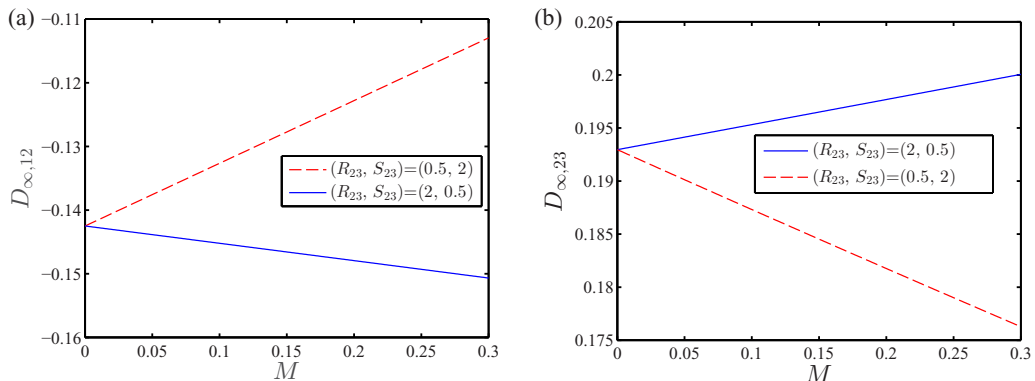


FIG. 5. Variation of D_∞ (steady-state deformation) with M (Mason number) for (a) inner (b) outer droplet of a leaky dielectric system when Ca (capillary number) = 0.1, Re (Reynolds number) = 0.01, λ_{12} (viscosity ratio) = λ_{32} (viscosity ratio) = 1, K (radius ratio) = 0.5, R_{12} (conductivity ratio) = $(R_{23})^{-1}$, and S_{12} (permittivity ratio) = $(S_{23})^{-1}$. Here, $R_{ij} = \sigma_i/\sigma_j$, $S_{ij} = \varepsilon_i/\varepsilon_j$, and $\lambda_{ij} = \mu_i/\mu_j$, where $(ij) \in \{12, 23\}$. 1, 2, and 3 are used to denote the inner fluid, outer fluid, and suspending fluid, respectively. The viscosity, electrical conductivity, and electrical permittivity are denoted by μ , σ , and ε , respectively.

of uniaxial extensional flow ($M = 0$). This was the study of Stone and Leal [15]. Thereafter, on increasing the strength of the external electric field, the oblate deformation of the inner droplet enhances for $R_{12} > S_{12}$, whereas the magnitude of deformation decreases for $R_{12} < S_{12}$. However, Fig. 5(b) shows that prolate deformation of the outer droplet increases with M for $R_{23} > S_{23}$, whereas it decreases for $R_{23} < S_{23}$. Now, we have given explanations of the observed phenomenon. When a leaky dielectric system experiences the combined presence of background extensional flow and uniform electric field, along with the background flow-induced viscous stress, the system also experiences additional electric field-induced stresses: (i) normal electric stress and (ii) normal hydrodynamic stresses.

For $R_{23} > S_{23}$ and $R_{12} < S_{12}$, the electric field-induced stresses act in the direction of background flow-induced viscous stress and tries to deform the outer droplet (or inner droplet) into prolate (or oblate) configuration. With the increase in Mason number, the combined strength of normal electric stress and normal hydrodynamic stress increases that enhances the deformation of the outer and inner droplets.

However, for $R_{23} < S_{23}$ and $R_{12} > S_{12}$, the electric field-induced stresses act opposite to the viscous stress and tries to minimize its effect. With the rise in Mason number, the strength of the electric field-induced normal stress increases and the net normal traction on the interface decreases that reduces the magnitude of prolate deformation of the outer droplet and oblate deformation of the inner droplet.

For studying the droplet deformation beyond the small deformation limit, we have employed numerical simulation and shown the deformation of a leaky dielectric system for a vast range of Mason numbers in Fig. 6. Figure 6(a) shows the variation of droplet deformation with Mason number for a leaky dielectric system having $S_{23} > R_{23}$ and $S_{12} < R_{12}$. From Fig. 6(a), it is also obtained that the outer and inner droplets deform into prolate and oblate configuration, respectively, for lower values of M ($M < 2$). However, with increase in the Mason number, the deformation of both the droplets decreases and the sense of deformation is reversed at sufficiently higher values of M . Further increase in M again enhances the oblate and prolate deformation of the outer and inner droplets, respectively. Droplet shapes at different Mason numbers have been shown in the inset of Fig. 6(a). It is also interesting to note that both the inner droplet and outer droplets deform into prolate configuration at $M = 2$. The physical explanation of the above-observed behavior is now provided. For the present leaky dielectric system, the applied electric field-induced stresses

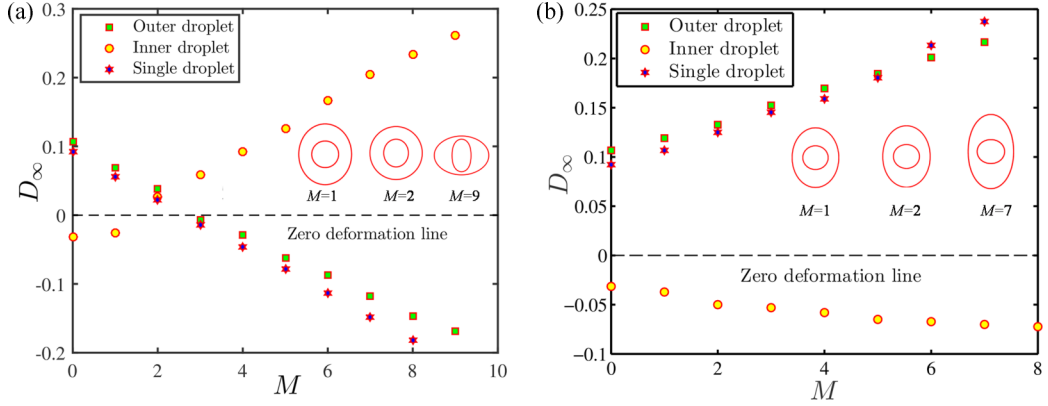


FIG. 6. Alteration of D_∞ (steady-state deformation) with M (Mason number) for different leaky dielectric systems having (a) $(R_{23}, S_{23}) = (0.5, 2)$, $(R_{12}, S_{12}) = (2, 0.5)$, where $R_{23} < S_{23}$ and $R_{12} > S_{12}$ and (b) $(R_{23}, S_{23}) = (2, 0.5)$, $(R_{12}, S_{12}) = (0.5, 2)$, where $R_{23} > S_{23}$ and $R_{12} < S_{12}$. The droplet shapes for different values of M are shown in the inset of Figs. 6(a) and 6(b). Important simulation parameters are capillary number (Ca) = 0.05, Reynolds number (Re) = 0.01, radius ratio (K) = 0.5, and viscosity ratio (λ_{12}) = (λ_{32}) = 1. Here, R_{ij} (conductivity ratio) = σ_i/σ_j , S_{ij} (permittivity ratio) = $\varepsilon_i/\varepsilon_j$ and λ_{ij} (viscosity ratio) = μ_i/μ_j , where $(ij) \in \{12, 23\}$. 1, 2, and 3 are used to denote the inner fluid, outer fluid, and suspending fluid. The viscosity, electrical conductivity, and electrical permittivity are denoted by μ , σ , and ε , respectively.

counteract the uniaxial extensional flow-induced droplet deformation. At lower values of M , the background uniaxial extensional flow is dominating. Hence, the outer droplet deforms into prolate and the inner droplet deforms into oblate configuration. However, at higher values of M , the electric field-induced deformation is more, which results in oblate and prolate configurations of the outer and inner droplets, respectively. One must acknowledge that there is a critical value of M , where the deformation of the droplet is zero. At the critical value of M , the combined effect of normal electric and hydrodynamic stresses is neutralized by uniaxial extensional flow-induced viscous stress.

Next, for showing the influence of an inner droplet on the deformation of the outer droplet for the present leaky dielectric system, we have made a comparison of the same with an equivalent single phase droplet in Fig. 6(a). From the figure, it is obtained that the deformation of the outer droplet is higher as compared to a single phase droplet for lower values of M . However, beyond the critical Mason number, the scenario is changed markedly where the deformation of the outer droplet is small in presence of the occluded droplet than without its presence. This occurs because of the fact that the presence of inner droplet increases the strength of fluid flow in the annular region. Therefore, the strength of the viscous stresses acting on the outer droplet is more than the single droplet. Because of that, the effect of electric field on the deformation of the outer droplet is less pronounced than the single droplet.

Figure 6(b) shows a similar study for a leaky dielectric system having $R_{23} > S_{23}$ and $R_{12} < S_{12}$. Figure 6(b) shows that the prolate (or oblate) deformation of outer droplet (or inner droplet) increases with increase in the Mason number. This can be explained by considering the fact that, for the present leaky dielectric system, the electric stress and viscous stress act along the same direction for both the inner and outer droplets. Therefore, the electric field aids the deformation of the inner and outer droplets due to extensional flow. Another important fact to note is that the enhancement of deformation of the outer droplet with Mason number is less than an equivalent single phase droplet. As $R_{12} < 1$, the induced surface charge at the interface is less and it produces a weak fluid flow circulation in the annular region. Since the fluid flow circulation in the annular region of the compound droplet due to the electric field is weak as compared to the equivalent single phase

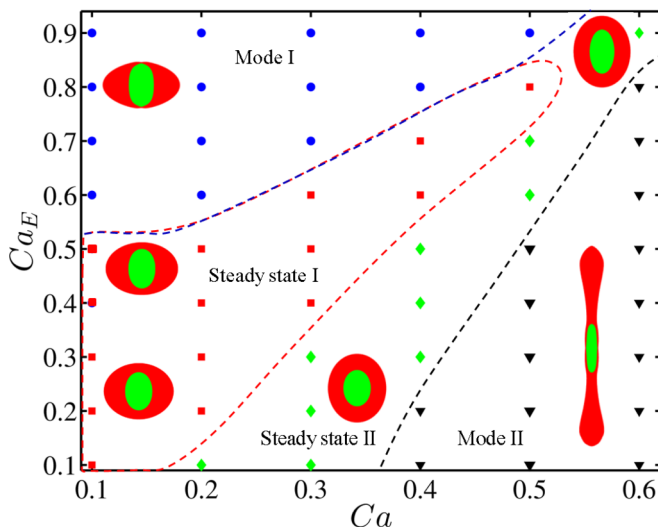


FIG. 7. Regime plot shows different patterns of droplet shape for different values of Ca (capillary number) and Ca_E (electric capillary number). Mode I: polar pinch-off; Mode II: equatorial pinch-off; Steady state I: Outer droplet is oblate shaped and inner droplet is prolate shaped; Steady state II: Both the droplets are prolate shape. Others parameters are $(R_{23}, S_{23}) = (0.5, 2)$, $(R_{12}, S_{12}) = (2, 0.5)$, K (radius ratio) = 0.5, Re (Reynolds number) = 0.01 and λ_{12} (viscosity ratio) = λ_{32} (viscosity ratio) = 1. Here, R_{ij} (conductivity ratio) = σ_i/σ_j , S_{ij} (permittivity ratio) = $\varepsilon_i/\varepsilon_j$, and λ_{ij} (viscosity ratio) = μ_i/μ_j , where $(ij) \in \{12, 23\}$. The viscosity, electrical conductivity, and electrical permittivity are denoted by μ , σ , and ε , respectively. 1, 2, and 3 are used to denote the inner fluid, outer fluid, and suspending fluid, respectively.

droplet, the enhancement of deformation because of electric field is also less for the outer interface of the compound droplet.

2. Electric field-modulated alteration in droplet morphology

This section is devoted toward understanding the combined influence of externally imposed electric field and extensional flow on the pinch-off dynamics of a compound droplet. Toward this, we investigate the role of two key parameters, namely Ca and Ca_E on the dynamics of the droplet. While Ca represents the relative strength of the imposed flow, the nondimensional parameter representing electric field strength is Ca_E . In sole presence of uniaxial extensional flow, the prolate (or oblate) deformation of the outer (or inner) droplet enhances with increase in the value of Ca (or shear rate) and beyond a critical value of it, the compound droplet undergoes pinch-off nucleating a hole at the equator (here, it is termed as “equatorial pinch-off”). This was the study of Stone and Leal (1990). Here, we have shown that the addition of the electric field alters this phenomenon markedly, where we have obtained four different patterns of droplet-shape-evolution across $Ca - Ca_E$ parameter space as discussed in the following paragraphs.

In contrast to the droplet configuration at lower values of Ca (< 0.2) reported in the study of Stone and Leal (1990), Fig. 7 shows that the presence of electric field creates the steady-state prolate (or oblate) deformation of the inner (or outer) droplet (steady state I) for moderate and higher values of Ca_E ($0.2 \leq Ca_E < 0.5$). However, if we further increase the value of Ca_E , beyond a critical value of it ($Ca_E \approx 0.55$), then the compound droplet undergoes pinch-off nucleating a hole at the pole, termed as “polar pinch-off” (mode I).

This phenomenon occurs due to the dominating nature of the electric field-induced stresses over the flow-induced viscous stress. In Fig. 8(a), we have shown the variation of E^2 with Ca_E . From the figure, it is evident that the magnitude of E^2 is higher at the poles for comparatively lower values

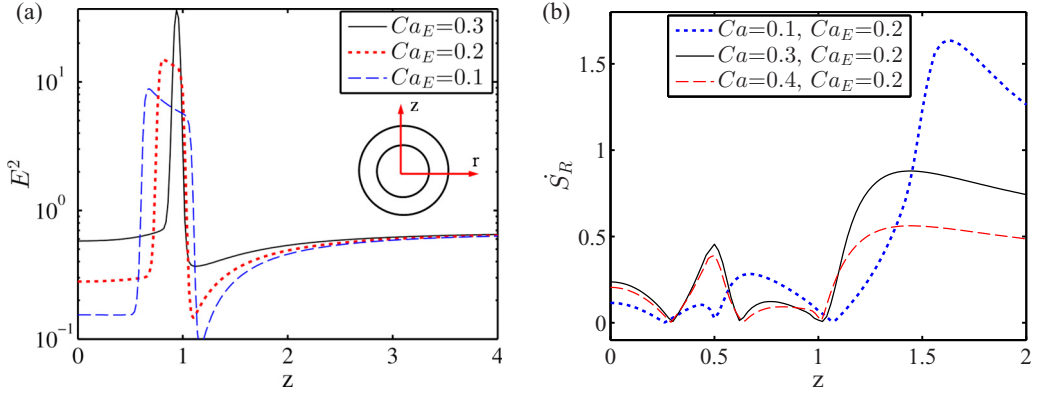


FIG. 8. Variation (a) E^2 (electric field squared) at Ca (capillary number) = 0.1 and (b) \dot{S}_R (shear rate) along a probe drawn from the center of the droplet to the upper electrode. Other parameters are $(R_{23}, S_{23}) = (0.5, 2)$, $(R_{12}, S_{12}) = (2, 0.5)$, K (radius ratio) = 0.5, Re (Reynolds number) = 0.01, and λ_{12} (viscosity ratio) = $\lambda_{32} = 1$. Here, R_{ij} 's (conductivity ratio) = σ_i/σ_j , S_{ij} (permittivity ratio) = $\varepsilon_i/\varepsilon_j$, and λ_{ij} (viscosity ratio) = μ_i/μ_j , where $(ij) \in \{12, 23\}$. 1, 2, and 3 are used to denote the inner fluid, outer fluid, and suspending fluid, respectively. The viscosity, electrical conductivity, and electrical permittivity are denoted by μ , σ , and ε , respectively.

of Ca_E , which necessarily means that the magnitude electric field-induced stress ($\sim E^2$) is also high that creates the steady state I configuration of the droplets. Now as we increase the value of Ca_E , the strength of the electric field-induced stress also increases which leads to the pinch-off of the droplet.

If we raise the magnitude of Ca , at the moderate value of $Ca(=0.3)$ and $Ca_E(=0.2)$, we have found that the droplet attains a different steady-state configuration (steady state II), where both the droplets deform into prolate shape. This phenomenon happens due to the fact that the magnitude of viscous stress increases with the enhancement of Ca as shown in Fig. 8(b), where we have depicted the variation of shear rate with the capillary number. From the figure, it is obtained that the shear rate at the droplet's tip enhances with the rise in the value of Ca that necessarily means that the viscous stress also increases and it attempts to reduce the effect electric field-induced stresses. Now, the effect of viscous stress is more significant in the case of outer droplet due to higher curvature. Thus, it reverses the pattern of deformation of the outer droplet. However, the electric field-induced stresses are still dominating for the inner droplet and creates the prolate deformation of the droplet. Here, one point needs to mention that the study of Stone and Leal [15] showed the equatorial pinch-off of the droplet for the same value of Ca in absence of electric field. Thus, we can say that the presence of electric field increases the critical capillary number which is of utmost importance in the design of emulsifier.

Keeping the value of Ca fixed, for the further enhancement in the values of $Ca_E(0.4 \leq Ca_E \leq 0.6)$, we have observed that the compound droplet system achieves steady state I configuration, where the outer droplet deforms into oblate configuration and the inner droplet deforms into prolate configuration. The reason behind this phenomenon is that the magnitude of electric field-induced stresses increases with the enhancement in the values of Ca_E that nullifies the effect of viscous stress due to background flow and creates the oblate deformation of the outer droplet. The additional increase in the value of $Ca_E(>0.6)$ leads to the polar pinch-off of the system (mode I). The significant enhancement of the electric field-induced stress at very higher values Ca_E is responsible for the polar pinch-off of the compound droplet system.

If we again raise the value of Ca to a great extent, at a very higher value of $Ca(=0.6)$ and moderate value of $Ca_E(=0.3)$, we observe equatorial pinch-off of the compound droplet system. This is due to the significantly higher strength of the flow-induced viscous stress. Under this condition, for additional raise in the values of $Ca_E(>0.8)$, we have obtained that the equatorial

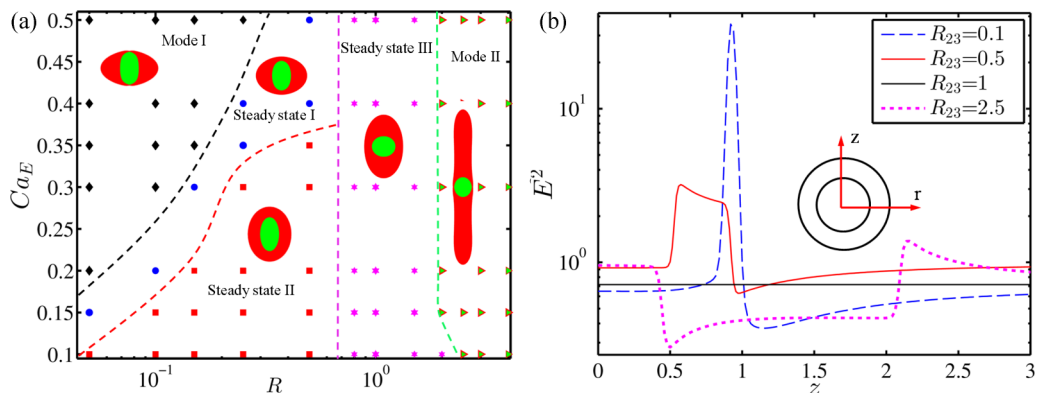


FIG. 9. (a) Regime plot shows different patterns of droplet breakup for different values of Ca_E (electric capillary number) and R (conductivity ratio). Mode I: polar pinch-off; Mode II: equatorial pinch-off; Steady state I: Outer droplet is oblate shaped and inner droplet is prolate shaped; Steady state II: Both the droplets are prolate shape; Steady state III: Outer droplet is prolate shaped and the inner droplet is oblate shaped. (b) Variation E^2 (electric field squared) along a probe drawn from the center of the droplet to the upper electrode. Others parameters are S_{23} (permittivity ratio) = 2, Ca (capillary number) = 0.35, λ (viscosity ratio) = 1, Ca_E (electric capillary number) = 0.15, K (radius ratio) = 0.5, Re (Reynolds number) = 0.01, $(R) = R_{23} = (R_{12})^{-1}$ and $S_{23} = (S_{12})^{-1}$. Here, R_{ij} (conductivity ratio) = σ_i/σ_j , S_{ij} (permittivity ratio) = $\varepsilon_i/\varepsilon_j$ and λ_{ij} (viscosity ratio) = μ_i/μ_j , where $(ij) \in \{12, 23\}$. 1, 2, and 3 are used to denote the inner fluid, outer fluid, and suspending fluid, respectively. The viscosity, electrical conductivity, and electrical permittivity are denoted by μ , σ , and ε , respectively.

pinch-off phenomenon has been suppressed and the compound droplet system achieves steady-state configuration. This happens because of the fact that the strength of the electric field-induced normal electric and hydrodynamic stresses increase, so as to suppress the pinch-off phenomenon by minimizing the effect of background flow-induced viscous stress.

3. Effect of electrophysical properties on the alteration of droplet morphology

This section is devoted to study the effect of electrophysical property variations (electrical conductivity, R) on the morphological characteristic of the compound droplet system as shown in Fig. 9(a). In the numerical analysis, the inner phase and the suspending fluid phase are considered to be the same. Hence, for convenience, we have chosen symbol R in the plots to represent the conductivity ratio of the system, where $R = R_{23} = 1/R_{12}$. For this analysis, we have considered a leaky dielectric system having higher values of Ca and we have performed large numbers of simulations to understand how droplet morphology alters across R - Ca_E space and we have discussed the characteristics in the following paragraphs.

At lower values of Ca_E ($=0.15$), we have obtained four different configurations of the compound droplet system depending on the values of R . At lower values of R (<0.1), we have obtained steady state I configuration, where the outer droplet deforms into oblate configuration and the inner droplet deforms into prolate configuration. Now, if we slightly increase the values of R ($0.1 \leq R < 0.8$), we have found that the droplet characteristic gets changed markedly and the droplet achieves steady state II configuration, where both the droplets deform into prolate configuration. Now if we further raise the values of R ($0.8 \leq R < 2$), we have seen that the outer droplet still deforms into prolate configuration but the inner droplet deforms into oblate configuration. Finally, the compound droplet undergoes equatorial pinch-off for increase in the values of R to a large extent ($R \geq 2$). This phenomenon can be explained from Fig. 8(b), where we have shown the variation of E^2 with R . From the figure, it is evident that the magnitude of E^2 is higher at the poles for lower values of R ,

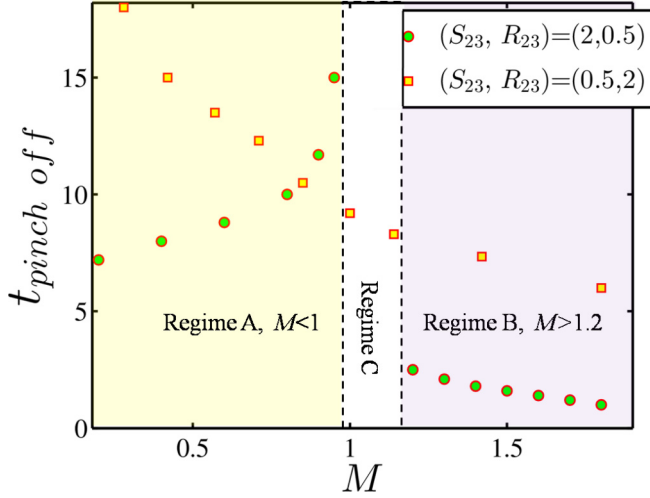


FIG. 10. Influence of electric field on the pinch-off time of the droplet. Others parameters are R_{23} (conductivity ratio) = $(R_{12})^{-1}$ and S_{23} (permittivity ratio) = $(S_{12})^{-1}$, λ_{12} (viscosity ratio) = $\lambda_{32} = 1$, K (radius ratio) = 0.5, Ca (capillary number) = 0.35, and Re (Reynolds number) = 0.01. Here, $R_{ij} = \sigma_i/\sigma_j$, $S_{ij} = \varepsilon_i/\varepsilon_j$, and $\lambda_{ij} = \mu_i/\mu_j$, where $(ij) \in \{12, 23\}$. 1, 2, and 3 are used to denote the inner fluid, outer fluid, and suspending fluid. The viscosity, electrical conductivity, and electrical permittivity are denoted by μ , σ , and ε , respectively.

which necessarily means that the magnitude electric field-induced stress ($\sim E^2$) is also high. In this regime, the electric field-induced stresses become dominating over the background flow-induced viscous stress and cause the oblate (or prolate) deformation of the outer (or inner) droplets. If we again increase the values of R , Fig. 9(b) shows that the strength of E^2 reduces. Therefore, the strength of electric stress also decreases and the viscous stress tries to dominate. The effect of viscous stress is more prominent for the outer droplet due to higher curvature and it creates prolate deformation of the outer droplet. However, the inner droplet still deforms into prolate configuration. If we further increase the values of R , we will find that the magnitude of E^2 becomes very small. In this regime, the flow-induced viscous stress governs the deformation characteristic and creates prolate (or oblate) deformation of the outer (or inner) droplet. For further enhancement of the values of R , we see that the magnitude of electric field-induced stresses increases. But in this regime, they act in the direction of viscous stress and create drastic elongation of the droplet, which finally leads to equatorial pinch-off.

Next, we slightly increase the value of Ca_E . At moderate values of Ca_E ($=0.30$) and lower values of R (<0.1), a polar pinch-off is also obtained in addition to the configurations observed when the values of Ca_E and R are low. This happens due to the fact that the magnitude of E^2 increases with Ca_E and its magnitude is quite high at moderate values of Ca_E as we discussed in Fig. 8(a). Therefore, the strength of the electric field-induced stresses is also more which causes the additional polar pinch-off of the droplet.

For very higher values of Ca_E ($=0.45$), it is interesting to note that the steady state II configuration of the compound droplet system vanishes and the configuration of the droplet is directly converted from steady state I to steady state III with increase in the values of R . Higher strength of electric stress at higher values of Ca_E is responsible for this behavior.

Next, we have investigated how the pinch-off time changes with Mason number (or Ca_E as the Ca is fixed) for different electrophysical properties. Figure 10 shows that the pinch-off time decreases with increase in the Mason number for the leaky dielectric system having $R_{23} > S_{23}$ and $R_{12} < S_{12}$. For this leaky dielectric system, the electric field-induced stresses act in the direction

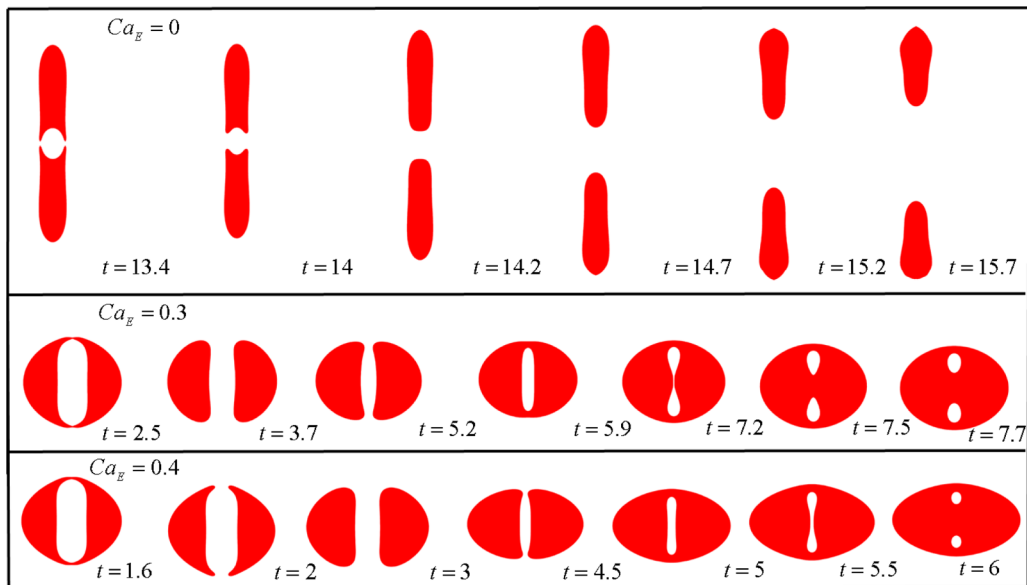


FIG. 11. Influence of electric field on the post pinch-off behavior of the droplet. Others parameters are $(R_{23}, S_{23}) = (0.1, 2)$, $(R_{12}, S_{12}) = (10, 0.5)$, Ca (capillary number) = 0.35, K (radius ratio) = 0.5, Re (Reynolds number) = 0.01, and viscosity ratio $(\lambda_{12}) = \lambda_{32} = 1$. Ca_E is the electric capillary number. Here, R_{ij} (conductivity ratio) = σ_i/σ_j , S_{ij} (permittivity ratio) = $\varepsilon_i/\varepsilon_j$, and λ_{ij} (viscosity ratio) = μ_i/μ_j , where $(ij) \in \{12, 23\}$. 1, 2, and 3 are used to denote the inner fluid, outer fluid, and suspending fluid. The viscosity, electrical conductivity, and electrical permittivity are denoted by μ , σ , and ε , respectively.

of viscous stress and their combined strength determines the pinch-off instances. With increase in M , the strength of electric field-induced stresses increases that causes the faster pinch-off of the system. However, for leaky dielectric system having $R_{23} < S_{23}$ and $R_{12} > S_{12}$, we have obtained three regimes: (i) in regime A having $M < 1$, the pinch-off time increases with increase in the values of M , (ii) in regime B having $M > 1.2$, the pinch-off time decreases with increase in the Mason number and (iii) regime C, where no pinch-off is observed. For the present leaky dielectric system, the electric field-induced stresses act in the opposite direction of the viscous stress and try to reduce its effect. In regime A, at very lower values of M , the pinch-off dynamics of the compound droplet system occurs due to the dominating natures of the background flow-induced viscous stress. As we increase the values of M , the strength of electric field-induced stresses increases that reduces the effect of viscous stress and delays the pinch-off phenomenon. In this regime, the maximum pinch-off time is obtained at $M = 0.95$.

However, in regime B, the pinch-off phenomenon is governed by the strength of electric field-induced stresses. Now in this regime, if we increase the values of M , the strength of the electric field induces stresses also increases that create faster pinch-off the droplets.

4. Effect of electric field on the post pinch-off behavior of the droplet

In Fig. 11, we show the effect of electric field on post pinch-off dynamics of the compound droplet system subjected to uniaxial extensional flow. From the figure, we can see that, in absence of electric field, after equatorial pinch-off, the daughter droplets move away from each other and try to achieve spherical configuration. However, the scenario changes completely in the presence of electric field. In the presence of electric field, after polar pinch-off, the interfaces of the outer shell at the poles again merge and form an elongated inner droplet. As time passes, the inner droplet tries to relax and undergoes midpoint break-up forming two spherical shaped daughter droplets. Further,

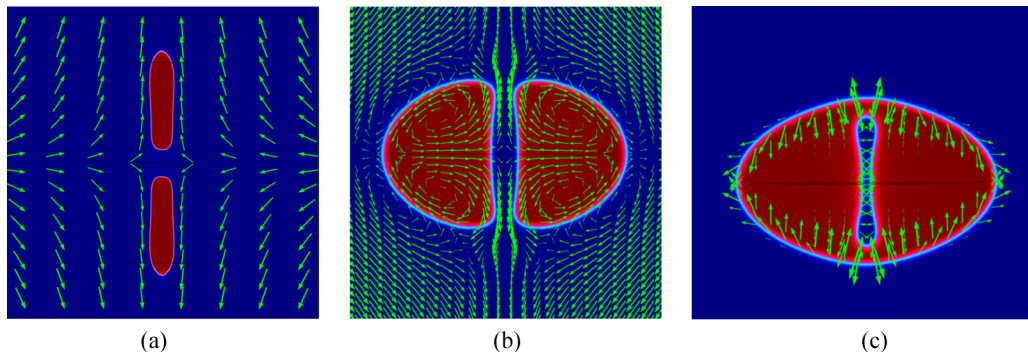


FIG. 12. Distribution of (a) uniaxial extensional flow at Ca_E (electric capillary number) = 0, (b) EHD flow at $Ca_E = 0.4$, (c) electric force distribution at $Ca_E = 0.4$. The arrow size denotes the strength of the respective variable. Other parameters are $(R_{23}, S_{23}) = (0.1, 2)$, $(R_{12}, S_{12}) = (10, 0.5)$, Ca (capillary number) = 0.35, K (radius ratio) = 0.5, Re (Reynolds number) = 0.01, and λ_{12} (viscosity ratio) = $\lambda_{32} = 1$. Here, R_{ij} (conductivity ratio) = σ_i/σ_j , S_{ij} (permittivity ratio) = $\varepsilon_i/\varepsilon_j$, and λ_{ij} (viscosity ratio) = μ_i/μ_j , where $(ij) \in \{12, 23\}$. The viscosity, electrical conductivity, and electrical permittivity are denoted by μ , σ , and ε , respectively. 1, 2, and 3 are used to denote the inner fluid, the outer fluid, and the suspending fluid.

if we increase the strength of electric field, then the post pinch-off behavior of the droplet remains the same; however, the size of the daughter droplet decreases.

We now provide a detailed explanation of the observed behavior. In sole presence of uniaxial extensional flow ($Ca_E = 0$), the equatorial pinch-off phenomenon is governed by the flow-induced viscous stress that drags the daughter droplets in the direction of flow as shown in Fig. 12(a). However, the polar pinch-off occurs as a result of the normal electric and hydrodynamic stresses induced by a strong electric field. After polar pinch-off, the outer shell is again reorganized due to the background viscous drag and electric field-induced flow and it entraps certain volume of suspending fluid in it. Initially, the inner fluid remains as elongated droplet and the electric stresses acting on its poles are tensile in nature. These stresses try to elongate the droplet in the direction of electric field. However, these electric stresses are compressive in nature at the equator and attempt to reduce the radius of the circular cross-section as shown in Fig. 12(b). However, the capillary stress again tries to convert the elongated droplet shape into spherical configuration

As the strength of the electric field-induced stresses is more (due to higher value of Ca_E), it first creates a neck at the equator which finally leads to mid-point break-up of the inner droplet forming two equal-sized daughter droplet. At a comparatively higher value of Ca_E , after pinch-off, the oblate deformation of the outer shell increases (elongated in the direction perpendicular to electric field) that decreases the volume of the entrapped fluid. Therefore, the size of the daughter droplet also reduces.

C. Effective viscosity of the dilute double emulsion

1. Effect of shape deformation: The role of electrophysical properties of the inner droplet

In this section, we analytically show how the electrical properties of the inner droplet affect the bulk rheology of the double emulsion in the combined presence of uniaxial extensional flow and uniform electric field. The effective extensional viscosity of a fluid characterizes the response of the fluid to externally applied tensile or elongational stress. According to the study of Stone and Leal (1990), the effective extensional viscosity of a compound droplet can be expressed as a function of radius ratio (K) and viscosity ratio (λ_{12} and λ_{23}) in absence of electric field. However, when electric field is applied, the electrophysical properties of the inner droplet plays a prime role in the alteration

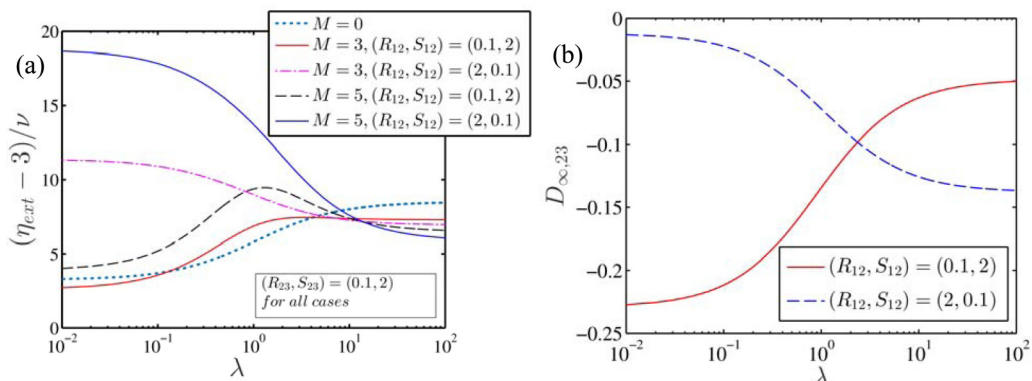


FIG. 13. Variation of extensional viscosity with viscosity ratio for leaky dielectric having Ca (capillary number) = 0.1. (b) Deformation of the outer interface ($D_{\infty,23}$) vs. viscosity ratio (λ) for the leaky dielectric system at M (Mason number) = 3. Other parameters are $(R_{23}, S_{23}) = (0.1, 2)$, K (radius ratio) = 0.5, Ca (capillary number) = 0.1, and Re (Reynolds number) = 0.01, λ (viscosity ratio) = $\lambda_{12} = \lambda_{23}$. Here, R_{ij} (conductivity ratio) = σ_i/σ_j , S_{ij} (permittivity ratio) = $\varepsilon_i/\varepsilon_j$, and λ_{ij} (viscosity ratio) = μ_i/μ_j , where $(ij) \in \{12, 23\}$. 1, 2, and 3 are used to denote the inner fluid, outer fluid, and suspending fluid. The viscosity, electrical conductivity, and electrical permittivity are denoted by μ , σ , and ε , respectively.

of the effective viscosity of the emulsion through the control of (i) the EHD flow that interacts with the flow created by the background extensional flow and (ii) the deformation of the outer droplets.

As our main focus is to study the impact of the electrical properties of the inner droplet, we have drawn the plots for different values of R_{12} and S_{12} keeping R_{23} and S_{23} constant. We have also assumed that the ratio of the viscosity of inner to annular phase is identical with the viscosity ratio between the annular and carrier phases ($\lambda = \lambda_{12} = \lambda_{23}$). Figure 13(a) shows that, in absence of external electric field, the magnitude of η_{ext} increases with increase in the value of λ . The reason is that highly viscous inner and annular fluid reduces the strength of fluid flow in and around the outer interface significantly that enhances the rate of dissipation in flow. However, the situation gets changed in the presence of electric field that is discussed in the following paragraphs.

For a leaky dielectric system having $R_{12} > S_{12}$, at lower values of λ (≤ 0.1), the effective extensional viscosity of the emulsion becomes quite large in presence of electric field (as compared to $M = 0$ case) and it decreases steadily as the magnitude of λ increases. This can be explained by the fact that, for the present system, the direction of the EHD flow is such that it opposes the externally imposed flow [27] and tries to create a very high magnitude of η_{ext} at lower values of λ . However, Fig. 13(b) shows that the oblate deformation of the outer droplet is small at lower values of λ for the considered electrical properties of the inner droplet ($R_{12} > S_{12}$). Hence, the contribution of shape deformation toward increasing η_{ext} can well be neglected. Therefore, the effect of EHD flow is most prominent toward dictating the extensional viscosity for a double emulsion at lower values of viscosity ratio. Another important fact is that the magnitude of η_{ext} increases on enhancing the value of M at lower values of λ , however, the scenario gets changed for higher values of λ (> 1), where magnitude of η_{ext} decreases with increase in the values of M . At lower values of λ , the strength of the EHD flow increases with increase in the values of M , resulting in a greater opposition to the incipient flow, thereby leading to a greater extensional viscosity. At higher values of λ , the EHD flow is suppressed, therefore the variation in η_{ext} occurs primarily due to the dominating effect of shape deformation. Because of the fact that the deformation of the droplets decreases with increase in the values of M , the magnitude of η_{ext} also reduces in the regime of higher values of λ .

For leaky dielectric system with $R_{12} < S_{12}$, at lower values of the λ (≤ 0.1), we find that the effective viscosity of the system decreases with slight increase in the values of M ($=3$). Further increase in the values of M ($=5$) again increases the values of η_{ext} . This happens due to the intricate

interplay of the shape deformation and EHD flow on the bulk rheology. For $R_{12} < S_{12}$, the EHD flow in the region exterior to the outer interface takes place from the equator to poles, thereby aiding the uniaxial extensional flow [27]. However, at the same time we can note [from Fig. 13(b)] that, for low values of the viscosity ratio, the outer droplet deforms by a large amount. Hence the effects of EHD flow and shape deformation counteract each other and the end result is that the effective viscosity first decreases and then increases with increase in the electric field strength. Figure 13(a) also reveals that the effective viscosity increases with increase in λ and attains a peak value when all three fluid media have almost the same viscosity ($\lambda \approx 1$). For further increase in viscosity ratio ($\lambda > 1$), the extensional viscosity decreases and attains a steady value. This happens due to the fact that, as the value of λ increases, the strength of the EHD flow is reduced, which is expected to increase the value of η_{ext} (as the EHD flow aids the incipient flow). However, Fig. 13(b) illustrated that, as λ increases, the magnitude of deformation of the outer droplet reduces which results in less opposition to the imposed flow thereby serving to decrease the value of η_{ext} . Hence when $R_{12} < S_{12}$, as λ is increased the EHD flow tries to increase η_{ext} , whereas shape deformation tries to reduce the value of η_{ext} . The effect of EHD flow dominates when the viscosity ratio is less than unity and we observe a steady increase in the value of η_{ext} . However, at $\lambda \approx 1$, the shape deformation of the outer droplet decreases sharply leading to a sharp change in the behavior of the extensional viscosity. Thereafter, on increasing the value of the viscosity ratio, the extensional viscosity of the double emulsion decreases and attains a steady value for large values of the viscosity ratio.

VI. CONCLUSIONS

In summary, we have revealed several nontrivial features related to shape evolution of the compound droplet in the combined presence of electric field and uniaxial extensional flow. These results may found importance in a multitude of engineering applications, ranging from manufacturing to microfluidics [51–60]. Furthermore, we have also made an attempt to explore the effect of the electrophysical properties of the inner droplet on the emulsion rheology of the dilute double emulsion. To accomplish this, we have developed an analytical solution for the deformation of the compound droplet as well as the emulsion rheology of the system valid within low deformation limit. To address some unexplored nonintuitive features related to the large distortion of the droplet, we have performed numerical simulations. Major findings of the present analysis are given below,

(i) In uniaxial extensional flow, the inner droplet deforms into oblate and the outer droplet deforms into prolate configuration. However, in the presence of electric field, we have obtained different shape-evolution patterns of the compound droplet system across Ca_E - R_{23} and Ca_E - Ca spaces. The patterns are: steady state I: Outer droplet is oblate shaped and inner droplet is prolate shaped; steady state II: Both the droplets are prolate shaped; steady state III: Outer droplet is prolate shaped and the inner droplet is oblate shaped. Besides that, two different modes of droplet pinch-off are also observed: Mode I: polar pinch-off; Mode II: equatorial pinch-off.

(ii) The pinch-off time is also found to be a strong function of electric field strength. For $R_{23} > S_{23}$ and $R_{12} < S_{12}$, the pinch-off time decreases monotonically with the strength of electric field. However, it shows the nonmonotonic variation with electric field strength for $R_{23} < S_{23}$ and $R_{12} > S_{12}$.

(iii) The presence of electric field also drastically alters the post pinch-off behavior of the droplet. On contrary to the sole effect of uniaxial extensional flow, after pinch-off, the interface of the outer shell again reunited in presence of electric field and formed a cylindrical inner droplet. As time passes, this inner droplet undergoes midpoint break-up creating two spherical inner daughter droplets. The size of the daughter droplet reduces as the strength of the electric field increases.

(iv) In presence of electric field, the effective extensional viscosity of the dilute double emulsion is altered with the electrophysical properties of the inner droplet in a nontrivial manner.

Because of very lengthy and complicated algebraic expressions of Φ_{ij} appearing in the analytical solution, we have not explicitly mentioned the detailed expressions here. The Maple program files

(.mw files) containing expressions of functions Φ_{ij} would be made available upon request to the corresponding author.

ACKNOWLEDGMENTS

S.S., D.P.P., and S.D. are grateful to Dr. Shubhadeep Mandal for insightful discussions on various numerical and mathematical intricacies. S.C. acknowledges Department of Science and Technology, Government of India, for Sir J. C. Bose National Fellowship.

S.S. and D.P.P. contributed equally to this work.

-
- [1] W. A. Macky, Some investigations on the deformation and breaking of water drops in strong electric fields, *Proc. R. Soc. A Math. Phys. Eng. Sci.* **133**, 565 (1931).
 - [2] C. G. Garton and Z. Krasucki, Bubbles in insulating liquids: Stability in an electric field, *Proc. R. Soc. A Math. Phys. Eng. Sci.* **280**, 211 (1964).
 - [3] S. L. Anna, Droplets and bubbles in microfluidic devices, *Annu. Rev. Fluid Mech.* **48**, 285 (2016).
 - [4] S.-Y. Teh, R. Lin, L.-H. Hung, and A. P. Lee, Droplet microfluidics, *Lab Chip* **8**, 198 (2008).
 - [5] Y. Zhu and Q. Fang, Analytical detection techniques for droplet microfluidics—A review, *Anal. Chim. Acta* **787**, 24 (2013).
 - [6] S. Mhatre, V. Vivacqua, M. Ghadiri, A. M. Abdullah, A. Hassanpour, B. Hewakandamby, B. Azzopardi, and B. Kermani, Electrostatic phase separation: A review, *Chem. Eng. Res. Des.* **96**, 177 (2015).
 - [7] M. J. Blanco-Prieto, E. Fattal, A. Gulik, J. C. Dedieu, B. P. Roques, and P. Couvreur, Characterization and morphological analysis of a cholecystokinin derivative peptide-loaded poly(lactide-co-glycolide) microspheres prepared by a water-in-oil-in-water emulsion solvent evaporation method, *J. Control. Release* **43**, 81 (1997).
 - [8] H. Okochi and M. Nakano, Preparation and evaluation of w/o/w type emulsions containing vancomycin, *Adv. Drug Deliv. Rev.* **45**, 5 (2000).
 - [9] A. Bozkir and G. Hayta, Preparation and evaluation of multiple emulsions water-in-oil-in-water (w/o/w) as delivery system for influenza virus antigens, *J. Drug Target.* **12**, 157 (2004).
 - [10] F. Courmarie, M.-P. Savelli, V. Rosilio, F. Bretez, C. Vauthier, J.-L. Grossiord, and M. Seiller, Insulin-loaded W/O/W multiple emulsions: Comparison of the performances of systems prepared with medium-chain-triglycerides and fish oil, *Eur. J. Pharm. Biopharm.* **58**, 477 (2004).
 - [11] J. Yan and R. Pal, Osmotic swelling behavior of globules of W/O/W emulsion liquid membranes, *J. Memb. Sci.* **190**, 79 (2001).
 - [12] H.-C. Kan, H. S. Udaykumar, W. Shyy, and R. Tran-Son-Tay, Hydrodynamics of a compound drop with application to leukocyte modeling, *Phys. Fluids* **10**, 760 (1998).
 - [13] S. Tasoglu, G. Kaynak, A. J. Szeri, U. Demirci, and M. Muradoglu, Impact of a compound droplet on a flat surface: A model for single cell epitaxy, *Phys. Fluids* **22**, 82103 (2010).
 - [14] J. F. Edd, D. Di Carlo, K. J. Humphry, S. Köster, D. Irimia, D. A. Weitz, and M. Toner, Controlled encapsulation of single-cells into monodisperse picolitre drops, *Lab Chip* **8**, 1262 (2008).
 - [15] H. A. Stone and L. G. Leal, Breakup of concentric double emulsion droplets in linear flows, *J. Fluid Mech.* **211**, 123 (1990).
 - [16] K. A. Smith, J. M. Ottino, and M. Olvera de la Cruz, Encapsulated Drop Breakup in Shear Flow, *Phys. Rev. Lett.* **93**, 204501 (2004).
 - [17] Y. Chen, X. Liu, and M. Shi, Hydrodynamics of double emulsion droplet in shear flow, *Appl. Phys. Lett.* **102**, 51609 (2013).
 - [18] R. E. Johnson and S. S. Sadhal, Fluid mechanics of compound multiphase drops and bubbles, *Annu. Rev. Fluid Mech.* **17**, 289 (1985).
 - [19] S. S. Sadhal and H. N. Oguz, Stokes flow past compound multiphase drops: The case of completely engulfed drops/bubbles, *J. Fluid Mech.* **160**, 511 (1985).

- [20] S. Mandal, U. Ghosh, and S. Chakraborty, Effect of surfactant on motion and deformation of compound droplets in arbitrary unbounded Stokes flows, *J. Fluid Mech.* **803**, 200 (2016).
- [21] X. Qu and Y. Wang, Dynamics of concentric and eccentric compound droplets suspended in extensional flows, *Phys. Fluids* **24**, 123302 (2012).
- [22] H. N. Gouz and S. S. Sadhal, Fluid dynamic and stability analysis of a compound droplet in an electric field, *Q. J. Mech. Appl. Math.* **42**, 65 (1989).
- [23] T. Tsukada, J. Mayama, M. Sato, and M. Hozawa, Theoretical and experimental studies on the behavior of a compound drop under a uniform DC electric field, *J. Chem. Eng. JPN.* **30**, 215 (1997).
- [24] J.-W. Ha and S.-M. Yang, Fluid dynamics of a double emulsion droplet in an electric field, *Phys. Fluids* **11**, 1029 (1999).
- [25] A. Behjatian and A. Esmaeeli, Transient electrohydrodynamics of compound drops, *Acta Mech.* **226**, 2581 (2015).
- [26] P. Soni, R. M. Thakkar, and V. A. Juvekar, Electrohydrodynamics of a concentric compound drop in an AC electric field, *Phys. Fluids* **30**, 32102 (2018).
- [27] A. Behjatian and A. Esmaeeli, Electrohydrodynamics of a compound drop, *Phys. Rev. E* **88**, 033012 (2013).
- [28] P. Soni, V. A. Juvekar, and V. M. Naik, Investigation on dynamics of double emulsion droplet in a uniform electric field, *J. Electrostat.* **71**, 471 (2013).
- [29] M. S. Abbasi, R. Song, J. Kim, and J. Lee, Electrohydrodynamic behavior and interface instability of double emulsion droplets under high electric field, *J. Electrostat.* **85**, 11 (2017).
- [30] M. S. Abbasi, R. Song, H. Kim, and J. Lee, Multimodal breakup of a double emulsion droplet under an electric field, *Soft Matter* **15**, 2292 (2019).
- [31] R. Pal, Multiple O/W/O emulsion rheology, *Langmuir* **12**, 2220 (1996).
- [32] F. N. Cogswell, Measuring the extensional rheology of polymer melts, *Trans. Soc. Rheol.* **16**, 383 (1972).
- [33] R. N. Shroff, L. V. Cancio, and M. Shida, Extensional flow of polymer melts, *Trans. Soc. Rheol.* **21**, 429 (1977).
- [34] S. Torza, R. G. Cox, and S. G. Mason, Electrohydrodynamic deformation and burst of liquid drops, *Philos. Trans. R. Soc. A Math. Phys. Eng. Sci.* **269**, 295 (1971).
- [35] G. Taylor, Studies in electrohydrodynamics. I. The circulation produced in a drop by electrical field, *Proc. R. Soc. A* **291**, 159 (1966).
- [36] D. A. Saville, Electrohydrodynamics: The Taylor-Melcher leaky dielectric model, *Annu. Rev. Fluid Mech.* **29**, 27 (1997).
- [37] M. N. Reddy and A. Esmaeeli, The EHD-driven fluid flow and deformation of a liquid jet by a transverse electric field, *Int. J. Multiph. Flow* **35**, 1051 (2009).
- [38] See Supplemental Material at <http://link.aps.org/supplemental/10.1103/PhysRevFluids.5.063602> for grid independence study, experimental relevance of assumptions, and methodology of our asymptotic analysis, which includes Refs. [27,34,35,37,45,46,61–73].
- [39] P. M. Vlahovska, On the rheology of a dilute emulsion in a uniform electric field, *J. Fluid Mech.* **670**, 481 (2011).
- [40] S. Mandal and S. Chakraborty, Uniform electric-field-induced nonNewtonian rheology of a dilute suspension of deformable Newtonian drops, *Phys. Rev. Fluids* **2**, 93602 (2017).
- [41] S. Mandal, S. Sinha, A. Bandopadhyay, and S. Chakraborty, Drop deformation and emulsion rheology under the combined influence of uniform electric field and linear flow, *J. Fluid Mech.* **841**, 408 (2018).
- [42] S. Mandal and S. Chakraborty, Effect of uniform electric field on the drop deformation in simple shear flow and emulsion shear rheology, *Phys. Fluids* **29**, 72109 (2017).
- [43] D. Barthès-Biesel, *Microhydrodynamics and Complex Fluids* (CRC Press, Boca Raton, FL, 2012).
- [44] N. Oba, H. Sugimura, Y. Umehara, M. Yoshida, T. Kimura, and T. Yamaguchi, Evaluation of an oleic acid water-in-oil-in-water-type multiple emulsion as potential drug carrier via the enteral route, *Lipids* **27**, 701 (1992).
- [45] S. Mandal, U. Ghosh, A. Bandopadhyay, and S. Chakraborty, Electroosmosis of superimposed fluids in the presence of modulated charged surfaces in narrow confinements, *J. Fluid Mech.* **776**, 390 (2015).

- [46] S. Santra, S. Mandal, and S. Chakraborty, Electrohydrodynamics of confined two-dimensional liquid droplets in uniform electric field, *Phys. Fluids* **30**, 62003 (2018).
- [47] D. Jacqmin, Calculation of two-phase Navier-Stokes flows using phase-field modeling, *J. Comput. Phys.* **155**, 96 (1999).
- [48] S. Santra, S. Mandal, and S. Chakraborty, Confinement effect on electrically induced dynamics of a droplet in shear flow, *Phys. Rev. E* **100**, 033101 (2019).
- [49] J.-W. Ha and S.-M. Yang, Deformation and breakup of Newtonian and non-Newtonian conducting drops in an electric field, *J. Fluid Mech.* **405**, 131 (2000).
- [50] A. Ramachandran and G. Leal, The effect of interfacial slip on the rheology of a dilute emulsion of drops for small capillary numbers, *J. Rheol.* **56**, 1555 (2012).
- [51] P. Mohan Raj, S. Sarkar, S. Chakraborty, G. Phanikumar, P. Dutta, and K. Chattopadhyay, Modelling of transport phenomena in laser surface alloying with distributed species mass source, *Int. J. Heat Fluid Flow* **23**, 298 (2002).
- [52] A. Ghatak and S. Chakraborty, Effect of external irreversibilities and variable thermal properties of working fluid on thermal performance of a dual internal combustion engine cycle, *Stroj. Cas. (Journal Mech. Energy)* **58**, 1 (2007).
- [53] S. P. Das, S. Chakraborty, and P. Dutta, Studies on thermal stratification phenomenon in LH₂ storage vessel, *Heat Transf. Eng.* **25**, 54 (2004).
- [54] S. Sarkar, P. M. Raj, S. Chakraborty, and P. Dutta, Three-dimensional computational modeling of momentum, heat, and mass transfer in a laser surface alloying process, *Numer. Heat Transf. Part A Appl.* **42**, 307 (2002).
- [55] N. Chakraborty and S. Chakraborty, Modelling of turbulent molten pool convection in laser welding of a copper-nickel dissimilar couple, *Int. J. Heat Mass Transf.* **50**, 1805 (2007).
- [56] R. Dua and S. Chakraborty, A novel modeling and simulation technique of photothermal interactions between lasers and living biological tissues undergoing multiple changes in phase, *Comput. Biol. Med.* **35**, 447 (2005).
- [57] S. Santra, D. Sen, S. Das, and S. Chakraborty, Electrohydrodynamic interaction between droplet pairs in a confined shear flow, *Phys. Fluids* **31**, 032005 (2019).
- [58] S. Chakraborty, Toward a generalized representation of surface effects on pressure-driven liquid flow in microchannels, *Appl. Phys. Lett.* **90**, 34108 (2007).
- [59] S. Das and S. Chakraborty, Transverse electrodes for improved DNA hybridization in microchannels, *AIChE J.* **53**, 1086 (2007).
- [60] P. Goswami, J. Chakraborty, A. Bandopadhyay, and S. Chakraborty, Electrokinetically modulated peristaltic transport of power-law fluids, *Microvasc. Res.* **103**, 41 (2016).
- [61] J. A. Lanauze, L. M. Walker, and A. S. Khair, The influence of inertia and charge relaxation on electrohydrodynamic drop deformation, *Phys. Fluids* **25**, 112101 (2013).
- [62] J. Zhang, J. D. Zahn, and H. Lin, Transient solution for droplet deformation under electric fields, *Phys. Rev. E* **87**, 043008 (2013).
- [63] J. C. Baygents, N. J. Rivette, and H. A. Stone, Electrohydrodynamic deformation and interaction of drop pairs, *J. Fluid Mech.* **368**, 359 (1998).
- [64] S. Mahlmann and D. T. Papageorgiou, Numerical study of electric field effects on the deformation of two-dimensional liquid drops in simple shear flow at arbitrary Reynolds number, *J. Fluid Mech.* **626**, 367 (2009).
- [65] A. Esmaeeli, Dielectrophoretic- and electrohydrodynamic-driven translational motion of a liquid column in transverse electric fields, *Phys. Fluids* **28**, 073306 (2016).
- [66] S. Mandal, A. Bandopadhyay, and S. Chakraborty, Dielectrophoresis of a surfactant-laden viscous drop, *Phys. Fluids* **28**, 062006 (2016).
- [67] O. Vizika and D. A. Saville, The electrohydrodynamic deformation of drops suspended in liquids in steady and oscillatory electric field, *J. Fluid Mech.* **239**, 1 (1992).
- [68] S. Santra, S. Das, and S. Chakraborty, Electrically modulated dynamics of a compound droplet in a confined microfluidic environment, *J. Fluid Mech.* **882**, A23 (2020).

- [69] E. Lac and G. M. Homsy, Axisymmetric deformation and stability of a viscous drop in a steady electric field, *J. Fluid Mech.* **590**, 239 (2007).
- [70] S. D. Deshmukh and R. M. Thaokar, Deformation and breakup of a leaky dielectric drop in a quadrupole electric field, *J. Fluid Mech.* **731**, 713 (2013).
- [71] X. Xu and G. M. Homsy, The settling velocity and shape distortion of drops in a uniform electric field, *J. Fluid Mech.* **564**, 395 (2006).
- [72] L. G. Leal, *Advanced Transport Phenomena* (Cambridge University Press, Cambridge, (2007).
- [73] S. Santra, S. Das, and S. Chakraborty, Electric field-induced pinch-off of a compound droplet in Poiseuille flow, *Phys. Fluids* **31**, 62004 (2019).